People's Democratic Republic of Algeria

Ministry of Higher Education and Scientific Research

University M'Hamed BOUGARA- Boumerdes

Institute of Electrical and Electronic

Engineering Department of Power and Control

Engineering

Project Report Presented in Partial Fulfilment of

the Requirements of the Degree of

'MASTER'

In Electrical and Electronic engineering

Option: Power Engineering

Title:

Improved Direct Torque Control of Switched Reluctance Motor 8/6 Using High Order Sliding Mode

Presented By:

- **Hicham GUEDIRI**
- **Mohammed Amin BOUKDIRA**

Supervisor:

Dr. AMMAR. A

Co-Supervisor:

Mr. CHEKNANE. A

June 2023

Dedication

I take immense pleasure and pride in dedicating this piece of work to those who have profoundly inspired and motivated me.

My heartfelt dedication goes out to my beloved parents and siblings, who truly deserve every ounce of gratitude.

Additionally, I extend my dedication to my fellow comrades in the university dormitory, with whom I experienced both joyful and challenging moments.

Last but not least, I express my appreciation to all my friends for their unwavering support and companionship throughout this journey.

Acknowledgements

First and foremost, I would like to express my gratitude to the Almighty, "Allah," for his blessings throughout this journey, as nothing occurs without his divine will.

I am sincerely thankful to my beloved parents and siblings whose encouragement, support, love, and unwavering dedication to my education have been invaluable. I am truly grateful for their presence in my life.

Secondly, I would like to convey my deepest appreciation and indebtedness to my honorable and esteemed supervisor, Dr. AMMAR Abdelkarim, from the Power and Control Engineering Department. His guidance, constructive criticism, and unwavering support have been instrumental not only during the course of this project but also throughout my time as his student. His insightful perspective on my work has been a constant source of inspiration, and I am fortunate to have the opportunity to collaborate with him. Additionally, I would like to express my sincere respect to my co-supervisor, CHEKNANE Abdelmalek, for his invaluable support and continuous guidance, regardless of the challenges encountered during this endeavor.

Lastly, I extend my heartfelt thanks to all those individuals who have directly or indirectly assisted me in the successful completion of this project.

Abstract

This research focuses on implementing a robust direct torque control (DTC) system for a Switched Reluctance Motor (SRM) by employing nonlinear approaches such as sliding mode control, Twisting controller (TC), and Super Twisting controller (STC). The initial phase involves the modeling of the SRM and its power supply, predominantly comprising a voltage inverter. Subsequently, the DTC technique is introduced and applied to the SRM. In the subsequent phase, two distinct control strategies, namely classical DTC and sliding mode DTC for SRM, are presented and discussed. Various numerical simulations are conducted to illustrate and explicate the effectiveness of these control techniques. In the final phase, Twisting and Super Twisting regulators are proposed with the intention of improving the chattering problem encountered in SRM control. The simulation results are subsequently presented to substantiate this assertion.

Keywords: Switched Reluctance Motor (SRM); Direct Torque Control (DTC); Sliding Mode Control (SMC); Chattering Phenomenon

Contents

Dedication ii

Acknowledgements iii

Abstract iv

List of Figures vii

List of Tables ix

List of Abbreviations x

Introduction xi

1 Description, Modeling and Supply of Switched Reluctance Motor (SRM) 1

1.1 Fundamental of Switched Reluctance Motor 2
1.1.1 Description of SRM 2
1.1.2 Torque – Speed Characteristics 3
1.1.3 Operation Principle of SRM 4
1.1.4 The Correlation Between Inductance and Rotor Position 5
1.2 Advantages and Disadvantages of SRM 6
1.2.1 Advantages 7
1.2.2 Disadvantages 7
1.3 Modeling of SRM 8
1.3.1 Torque Production in SRM 9
1.3.2 Mechanical Model (the motion equation) 10
1.4 Supply of The Switched Reluctance Motor 11
1.4.1 Energization of the phase of SRM 11
1.4.2 Asymmetric Half-Bridge Converter 11
1.5 Simulation of SRM with Current Loop Control 13
1.5.1 Simulation Results 13
1.6 Conclusion 15

2 Direct Torque Control for SRM Using PI Controller **16**
2.1 Direct Torque Control . . . 17
2.1.1 Bases of DTC Control . . . 17
2.1.1.1 Stator flux control principle . . . 17
2.1.1.2 Principle of electromagnetic torque control . . . 18
2.1.1.3 Estimation of flux . . . 19
2.1.1.4 Estimation of the electromagnetic torque . . . 20
2.1.2 Direct Torque Control Applied on SRM 8/6 . . . 21
2.1.2.1 Principle of DTC Applied on SRM 8/6 . . . 21
2.1.2.2 Speed regulation using PI controller . . . 24
2.2 Simulation and Results . . . 26
2.2.1 Block diagram of classic DTC . . . 26
2.3 Conclusion . . . 30

3 High Order Sliding Mode Control of SRM **31**
3.1 Sliding mode control . . . 31
3.1.1 Sliding surface choice . . . 32
3.1.2 Existence conditions of sliding mode . . . 33
3.1.3 Control design . . . 34
3.1.4 Chattering phenomenon . . . 35
3.1.5 Solutions to reduce the Chattering phenomenon . . . 36
3.1.5.1 Changing the switching function . . . 36
3.1.5.2 Solution by approach laws . . . 37
3.1.5.3 Solution by higher order sliding modes controllers . . . 37
3.2 Second order sliding mode control . . . 38
3.2.1 Control design . . . 38
3.2.2 Examples of second order sliding mode control . . . 39
3.2.3 Twisting algorithm . . . 39
3.2.4 Super Twisting algorithm . . . 40
3.2.5 Design of sliding mode controllers . . . 41
3.2.5.1 First order SM-speed controller design . . . 41
3.2.5.2 Twisting SM-speed controller design . . . 42
3.2.5.3 Super Twisting SM-speed controller design . . . 43
3.3 Simulation, Results, and Discussion . . . 44
3.3.1 Results of simulations . . . 44
3.4 Conclusion . . . 49

Conclusion & Future Plans **51**

Appendices **52**

Bibliography **53**

List of Figures

1.1 8/6 SRM structure . . . 2
1.2 Torque-speed curve of SRM . . . 3
1.3 Three phase SRM cross section: a) Unaligned rotor position, b) Aligned rotor position . . . 4
1.4 variation of inductance . . . 5
1.5 Optimal Phase Inductance under Rotor Position Variation . . . 5
1.6 The inductance profiles of the SRM's three phases . . . 6
1.7 Co-energy graph between aligned and unaligned rotor situations . . . 10
1.8 Mechanical drive of the motor system . . . 11
1.9 Typical diagram of the phase current for a VSSRM drive . . . 11
1.10 Four-phase asymmetric half-bridge converter . . . 12
1.11 Asymmetric half-bridge converter switching states. (a) Magnetization. (b)Demagnetization. (c) Freewheeling. . . . 12
1.12 Block diagram of current loop control of SRM . . . 13
1.13 Position Sensor . . . 13
1.14 One phase flux ripples . . . 14
1.15 Output current ripple of one phase . . . 14
1.16 Motor speed with load . . . 14
1.17 Torque ripple under load . . . 15

2.1 Stator flux vector trajectory. . . . 18
2.2 Two-level hysteresis controller for controlling the flux error. . . . 20
2.3 Three-level Hysteresis Controller for Control of Torque Error . . . 21
2.4 Definition of SRM motor voltage vectors for DTC . . . 22
2.5 Definition of 2- axis for motor voltage . . . 23
2.6 Speed regulation loop . . . 24
2.7 DTC with PI speed regulator for SRM . . . 26
2.8 Block diagram of DTC with PI regulator of SRM . . . 27
2.9 Flux and torque hysteresis controller plus sector determination . . . 27
2.10 Switching table . . . 28
2.11 Output current ripple of one phase . . . 28
2.12 One phase flux linkage ripple and the total stator flux vector . . . 29
2.13 Speed of the motor with zoom at the time of loading the motor . . . 29
2.14 Torque ripples . . . 30

3.1 Sliding mode principle of state trajectory. . . . 32
3.2 Equivalent control structure. . . . 34
3.3 The chattering phenomenon . . . 36

3.4 Saturation and sigmoid functions. 36
3.5 Twisting controller trajectory 40
3.6 Torque response for 1st Order Sliding Mode 44
3.7 Torque response for Twisting controller 45
3.8 Torque response for Super-Twisting controller 45
3.9 Speed response for 1st Order Sliding Mode 46
3.10 Speed response for Twisting controller 46
3.11 Speed response for Super-Twisting controller 46
3.12 Speed PI/1st order SM/Twisting SM/Super Twisting SM 47
3.13 Output current ripple of one phase for First Order Sliding Mode 47
3.14 Output current ripple of one phase for Twisting controller 47
3.15 Output current ripple of one phase for Super-Twisting controller 48
3.16 One phase flux linkage for 1st Order Sliding Mode 48
3.17 One phase flux linkage for Twisting controller 48
3.18 One phase flux linkage for Super-Twisting controller 49

List of Tables

1.1 The variation of inductance affects the production of torque 6
1.2 The comparison of SRM with other motors 8

2.1 Switching Logic for Flux error 20
2.2 Switching Logic for Torque Error 21
2.3 Switching Table of space voltage vectors 24

3.1 The different performances of each controller 49

List of Abbreviations

AC Alternating Current

DC Direct Current

DTC Direct Torque Control

HOSC High Order Sliding Mode Control

PM Permanent Magnet

PWM Pulse Width Modulation

SM Sliding Mode

SMC Sliding Mode Control

SRM Switched Reluctance Motor

STSMC Super Twisting Slinding Mode Control

TSMC Twisting Sliding Mode Control

VRM Variable Reluctance Motor

VSSRM Voltage Source Switched Reluctance Motor

Introduction

The Switched Reluctance Motor (SRM) has gained significant attention in both academic and industrial circles due to its simple construction and robust behavior, particularly in high-speed applications. Furthermore, SRMs exhibit high efficiency and require minimal maintenance. These advantages have positioned switched reluctance motor drives as a promising alternative to AC induction motor drives and permanent magnet synchronous motor drives in specific applications. The switched reluctance motor is an electrical machine that converts electric power into mechanical power. Similar to conventional motors like induction and synchronous motors, it can operate in all four quadrants, allowing for clockwise and anticlockwise rotor rotations [1].

Controlling the switched reluctance motor is not as straightforward as traditional machines. One crucial aspect of control is minimizing torque ripple, which has been extensively studied in the field [2]. Nonetheless, SRMs still face certain challenges that prevent their widespread use. The main issues include excessive acoustic noise caused by radial forces affecting the rotor and substantial torque ripple when stator currents are controlled using conventional PID-type controllers. Addressing the former problem can be achieved through appropriate machine design, while the latter necessitates the adoption of non-conventional control techniques [3].

The control complexity of SRMs has led to the development of various control strategies, with Direct Torque Control (DTC) being the most popular. DTC exhibits excellent performance during transient and steady-state phases. Initially, PID controllers were employed due to their simplicity and ease of implementation. However, they lack robustness when faced with variations in machine parameters. To accommodate a broader range of parameter variations and ensure robustness regardless of the operating point, a nonlinear control technique called variable structured control (VSC) or sliding mode control (SMC) has been widely adopted. VSC/SMC is known for its simplicity, speed, and robustness, demonstrating effectiveness in numerous applications.

Despite the aforementioned advantages, controllers utilizing variable structures suffer from a significant drawback known as chattering. To mitigate this issue while maintaining control robustness, various solutions have been proposed to strike a balance between reducing the chattering phenomenon and preserving control performance.

Based on these considerations, this study proposes a robust nonlinear control approach utilizing the Twisting controller (TC) and Super Twisting controller (STC) for switched reluctance motors under various conditions. The primary objective of employing Twisting and Super Twisting control in this work is to enhance the performance of sliding mode

control by minimizing the chattering phenomenon while retaining the desirable properties of the control mode.

The report is structured into three chapters as follows:

The initial chapter aims to provide a description, model, and supply of the Switched Reluctance Motor (SRM).

The second chapter is dedicated to the modeling and conventional Direct Torque Control (DTC) of the switched reluctance motor (SRM). The classical Proportional-Integral (PI) controller will be utilized. Various results from digital simulations of vector control will be presented and analyzed.

The final chapter focuses on the design of a sliding mode controller (SMC) for the SRM. Firstly, the design steps of the SMC will be thoroughly explained. To mitigate chattering phenomena, we propose the utilization of Twisting and Super Twisting control algorithms, also known as second-order sliding mode controllers for the SRM drive. Simulation results will be provided to validate this approach.

To conclude this study, a comprehensive summary will be presented, highlighting key observations and suggesting potential areas for future research in this field.

Chapter 1

Description, Modeling and Supply of Switched Reluctance Motor (SRM)

Introduction

Switched Reluctance Motors (SRMs) have attracted increasing attention from researchers worldwide due to their uncomplicated mechanical design and cost-effectiveness. Furthermore, the absence of permanent magnets or windings in the robust rotor enhances its fault-tolerant capability and enables efficient high-speed performance. Nevertheless, the inherent doubly salient structure and nonlinear magnetization characteristics of SRMs result in a significant output torque ripple, which imposes limitations on their broader application [4].

While the operational principles of SRMs are straightforward, achieving proper control of these motors remains a challenge. The inherent nonlinearity of SRMs means that torque production heavily relies on the pole geometry, which is influenced by both the stator current and rotor position [4][5].

In this chapter, we will provide an introduction to the switched reluctance motor, explaining its functionality, modeling, and power supply. Additionally, we will discuss the drawbacks of SRMs and present simulations to illustrate these limitations.

1.1 Fundamental of Switched Reluctance Motor

1.1.1 Description of SRM

A switched reluctance motor shares physical similarities with other rotating motors such as AC and DC varieties. For example, it resembles an induction motor or a DC-powered motor. Figure 1.1 illustrates the structure of an 8/6 pole SRM, which consists of two distinct components. Typically, the number of poles in the stator and rotor is different. Unlike other motor types, the windings in a switched reluctance motor are less complex. Only the stator poles have coils wound around them, while the rotor poles lack any winding. The number of phases formed by connecting opposite pole windings in parallel or series is exactly half of the stator poles. Consequently, a single phase excites two stator poles. The rotor has a simple laminated structure with protruding poles but no winding. This design offers the advantage of reducing copper loss in the rotor winding. In applications where higher efficiency is required, silicon steel is the preferred material for the rotor stampings. To accommodate the high-speed operation of the rotor in aerospace applications, cobalt and iron materials, along with other adjustments, are employed. Minimizing the air gap size, typically between 0.1 and 0.3mm, is a key consideration. It is considered optimal for the rotor pole arc to be approximately equal to the stator pole arc [6].

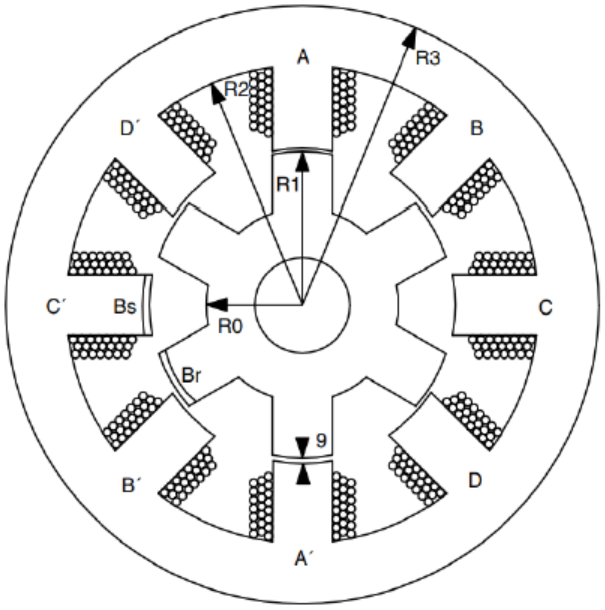

FIGURE 1.1: 8/6 SRM structure

1.1.2 Torque – Speed Characteristics

When utilizing electric machines under different circumstances, it is crucial to take into account various factors. However, the primary objective is to achieve the highest possible power output. An essential visual representation, as shown in Figure 1.2, is the torque-speed curve. This curve illustrates the performance of the machine in different operating conditions, demonstrating the connection between motor speed and its maximum torque at each speed. Furthermore, it provides information about the machine's maximum power output. Given that the equation defines the output of any electric machine:

$$P_{out} = T\omega \tag{1.1}$$

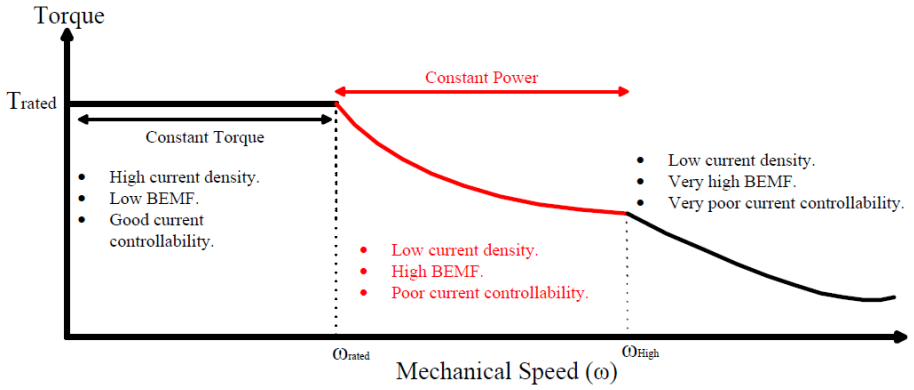

FIGURE 1.2: Torque-speed curve of SRM

The machine's output power, denoted as P_{out}, is determined by its mechanical torque (T) and rotor speed (ω). Different speed loadings impose various limitations and constraints on the machine's operation. At low speeds, the torque production is limited by the machine's thermal constraints, as it cannot withstand higher currents. On the other hand, at high speeds, the motor encounters restrictions due to the high back EMF voltage, which hampers current build-up.

Another constraint arises from the limited time available for the accumulation and discharge of electric current at fast rates. In the case of a synchronous motor like an SRM, the electrical cycle diminishes with an increase in motor velocity, leading to a shorter duration for current discharge.

This abbreviated electrical cycle often results in a residual current that extends into the negative torque region, thereby reducing the overall torque output of the machine. The main goal of this thesis is to tackle the challenge of efficiently discharging the current at higher speeds.

Improving the rate of current discharge can have positive effects on torque production by allowing for a longer magnetization time (higher turn-off), potentially increasing positive torque. Additionally, it can minimize negative torque production since the current will be reset to zero before entering the negative torque zones [7].

1.1.3 Operation Principle of SRM

Figure 1.3 presents a cross-sectional perspective of a three-phase switched reluctance motor (SRM). Smooth rotation is achieved by supplying the appropriate current to each phase winding at the corresponding rotor angle. The excitation occurs sequentially, transitioning from one phase to the next as the rotor rotates. The alteration in inductance throughout this process is depicted in Figure 1.4.

When the rotor poles R1 and R1´ align with the stator poles, the application of an electric current to the A phase winding results in magnetic flux passing through the A and A´ stator poles, as well as the R2 and R2' rotor poles. This generates an energy that attracts the rotor poles towards A and A´. Once the R2 and R2' poles align correctly with the stator poles, the current in phase A is deactivated, as illustrated in Figure 1.3 [8].

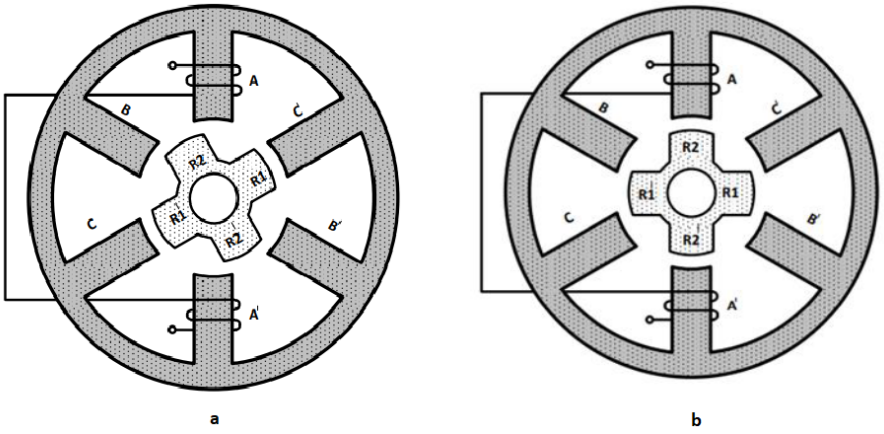

FIGURE 1.3: Three phase SRM cross section: a) Unaligned rotor position, b) Aligned rotor position

The SRM acquired its name due to the technique employed in rotor movement, which entails the converter switching process. This methodology functions based on the principle that when the rotor aligns with the stator poles, the space between them diminishes, leading to an elevation in inductance. This connection between the rotor and stator is the fundamental reason behind the SRM's designation.

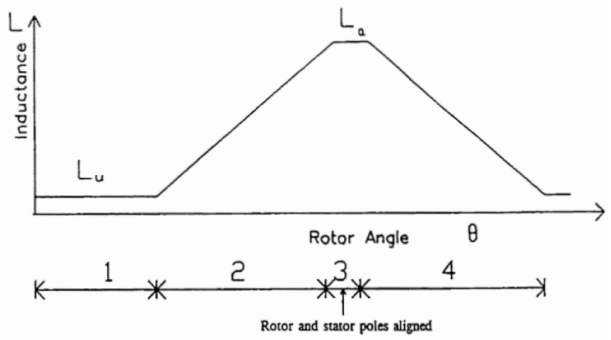

FIGURE 1.4: variation of inductance

1.1.4 The Correlation Between Inductance and Rotor Position

Figure 1.5 demonstrates the optimal change in phase inductance in relation to the rotor's location for a 6/4 switched reluctance motor (SRM).

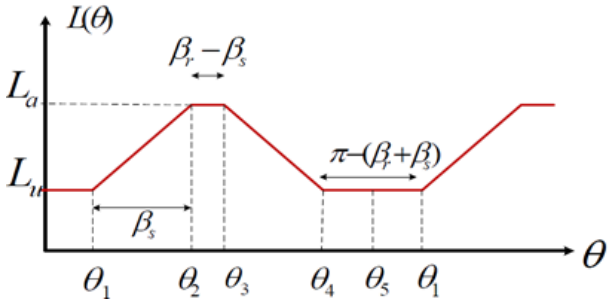

FIGURE 1.5: Optimal Phase Inductance under Rotor Position Variation

Where:

$$\theta_1 = \frac{1}{2}\left[\frac{2\pi}{N_r} - (\beta_s + \beta_r)\right] \tag{1.2}$$

$$\theta_2 = \theta_1 + \beta_s \tag{1.3}$$

$$\theta_2 = \theta_2 + (\beta_r - \beta_s) \tag{1.4}$$

$$\theta_4 = \theta_3 + \beta_s \tag{1.5}$$

$$\theta_5 = \theta_4 + \theta_1 = \frac{2\pi}{N_r} \tag{1.6}$$

Figure 1.6 illustrates the three-phase inductance profile of the 6/4 SRM.

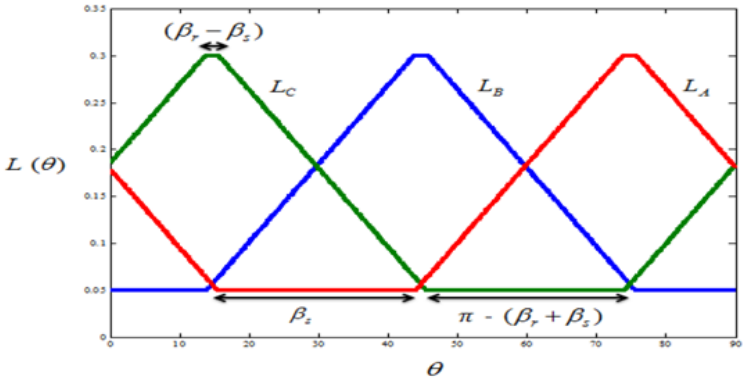

FIGURE 1.6: The inductance profiles of the SRM's three phases

TABLE 1.1: The variation of inductance affects the production of torque

Rotor Angles	Results
0 - θ_1 and θ_4 - θ_5	When there is no overlapping between rotor and stator leads to minimum inductance and no production of torque.
θ_1 - θ_2	Poles overlap, increasing of inductance with positive slope, a positive torque generation.
θ_2 - θ_3	If the Intersection in between the rotor stator remains unchanged and the inductance is maintained at its highest value, then there will be no production of torque.
θ_3 - θ_4	As the rotor pole moves further from overlapping, the inductance lowers, leading to a negative slope and negative torque production.

The basic concept of a switching reluctance motor has been illustrated in the simplified representation above. Nevertheless, practical motors will display a gradual change in the inductance profile across the transition regions owing to the magnetic saturation caused by a rise in flux density in the ferromagnetic material during the alignment of pole. Furthermore, there will be delays in the smooth rise of coil currents, leading to irregularities or fluctuations in the overall generation of electromagnetic torque.

1.2 Advantages and Disadvantages of SRM

In this section, we will present the strengths and weaknesses of the SRM resulting from its specific design.

1.2.1 Advantages

The SRM possesses distinct features that position it as a strong competitor to existing AC and DC motors in adjustable-speed drive and servo applications. The advantages of an SRM can be summarized as follows [9]:

- The construction of the machine is simple and cost-effective due to the absence of rotor winding and permanent magnets.
- There are no shoot-through faults between the DC buses in the SRM drive converter, as each rotor winding is connected in series with converter switching elements.
- The need for bidirectional currents is eliminated, thereby reducing the number of power switches required in certain applications.
- The majority of losses occur in the stator, which is comparatively easier to cool.
- The torque-speed characteristics of the motor can be easily customized to meet the specific requirements of the application during the design phase, in contrast to induction and PM machines.
- The SRM exhibits a high starting torque without the concern of excessive in-rush current, thanks to its elevated self-inductance.
- The occurrence of open-circuit voltage and short-circuit current during faults is minimal or negligible.
- The absence of permanent magnets allows for a higher maximum permissible rotor temperature.
- The SRM boasts a low rotor inertia and a favorable torque-to-inertia ratio.
- It is capable of achieving extremely high speeds while maintaining a wide constant power region.
- The independent stator phases enable continued operation of the drive even in the event of the loss of one or more phases.

1.2.2 Disadvantages

The SRM does have a few disadvantages, with torque ripple and acoustic noise being the most significant. The double saliency construction and the discrete nature of torque production by the independent phases contribute to higher torque ripple compared to other types of machines. This increased torque ripple also leads to a large ripple current in the DC supply,

necessitating a substantial filter capacitor. Additionally, the doubly salient structure of the SRM results in higher acoustic noise levels compared to other machines. The primary source of this noise is the radial magnetic force causing resonant vibrations with the circumferential mode shapes of the stator.

Furthermore, the absence of permanent magnets places the burden of excitation on the stator windings and converter, which increases the converter's kVA requirement. In comparison to PM brushless machines, the stator copper losses per unit will be higher, leading to reduced efficiency and torque per ampere. However, unlike PM machines, the maximum speed at constant power is not limited by fixed magnet flux, allowing for an extended constant power region of operation in SRMs. The control system for SRMs can be simpler than the field-oriented control used for induction machines, although significant computations may be necessary for minimizing torque ripple in an SRM drive [9].

TABLE 1.2: The comparison of SRM with other motors

	Induction Motor	**Synchronous Motor**	**DC Motor**	**Step Motor**	**SRM**
Supply voltage	Alternating voltage	Alternating voltage	Direct voltage	Direct voltage	Direct voltage
Excitation voltage	Not required	Direct voltage	Direct voltage	Not required	Not required
Driver	Necessary in variable speed applications	Necessary in variable speed applications	Necessary in variable speed applications	Always necessary	Always necessary
Operation and maintenance costs	Low	Average	Average	Low	Low
Cost	Low	High	High	Average	Average
Driver cost	High	High	High	Average	Average
Efficiency	Average	High	Average	Average	High

1.3 Modeling of SRM

When the interaction between phases is disregarded, the voltage across the phase terminals of a Switched Reluctance Motor (SRM) can be expressed by [10].

$$V = Ri + \frac{d\phi}{dt} \tag{1.7}$$

Where φ is the flux linkage and R is the stator winding resistance. Magnetic saturation can be taken into account, with the flux linkage being a function of both current and rotor position, θ. Flux linkage, therefore, can be defined as:

$$\varphi(\theta, i) = L(\theta, i) \cdot i(t) \tag{1.8}$$

Replacing (1.8) in (1.7) and calculating the flux linkage derivative, results

$$v = Ri + L(\theta, i)\frac{\partial \varphi}{\partial t} + i\frac{\partial L(\theta, i)}{\partial t} \tag{1.9}$$

When the derivative of the inductance with respect to time is expanded, the outcome is :

$$\frac{\partial L(\theta, i)}{\partial t} = \frac{\partial L(\theta, i)}{\partial t}\frac{d\theta}{dt} + \frac{\partial L(\theta, i)}{\partial i}\frac{di}{dt} \tag{1.10}$$

1.3.1 Torque Production in SRM

When a current, denoted as i_a in Figure 1.7, is applied while maintaining the rotor at a position θ_1 between the unaligned and aligned positions, the instantaneous electromagnetic torque can be calculated according to [8]. If the current i_a is kept constant while allowing the rotor to move incrementally from position θ_1 to $\theta_1 + \Delta\theta_{\text{mech}}$, the corresponding equation is derived:

$$\Delta W_{\text{mech}} = T_{\text{em}}\Delta\theta_{\text{mech}} \tag{1.11}$$

The incremental energy delivered by the electrical source is the equation:

$$\Delta W_{\text{elec}} = \text{area}(1 - \varphi_1 - \varphi_2 - 2 - 1) \tag{1.12}$$

Where 1 and 2 are flux linkages at two rotor positions. The area above is the incremental energy stored with corresponding winding so

$$\Delta W_{\text{storage}} = \text{area}(0 - 2 - \phi_2 - 0) - \text{area}(0 - 1 - \phi_1 - 0) \tag{1.13}$$

The mechanical work done is the difference between the electrical energy and energy stored

$$\Delta W_{\text{mech}} = \Delta W_{\text{elec}} - \Delta W_{\text{storage}} \tag{1.14}$$

Thus, the amount of mechanical work performed equates to the co-energy existing between two distinct positions of the rotor, namely position 1 and position 2. Consequently, the electromagnetic torque can be expressed as a dependent variable on both the rotor position

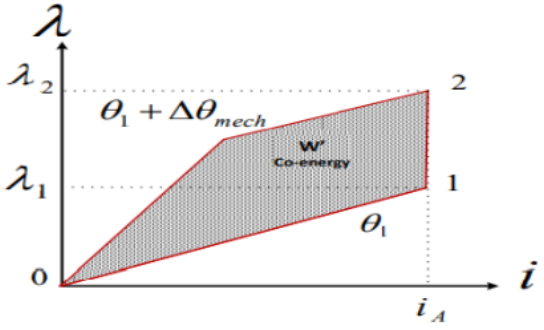

FIGURE 1.7: Co-energy graph between aligned and unaligned rotor situations

and the current.

$$T_e = \frac{\partial W'}{\partial \theta} \tag{1.15}$$

Considering the nonlinearity of torque with respect to both the phase current and rotor position, as illustrated in Figure 1.7, Equation (1.15) can be reformulated to represent the change in inductance from the unaligned position to the aligned position.

$$T_e = \frac{1}{2} i^2 \frac{dL}{d\theta} \tag{1.16}$$

1.3.2 Mechanical Model (the motion equation)

In order to regulate the speed of the Switched Reluctance Motor (SRM), it is necessary to consider the mechanical equations related to the load during the simulation process. By adopting this approach, the motor's speed performance can be analyzed both under loaded conditions and in the absence of any load. In the mechanical model, it is possible to incorporate the effects of friction within the system. The corresponding equation, can be expressed as follows [10]:

$$T_{\text{friction}} = B\omega \tag{1.17}$$

By utilizing the equation mentioned above, the equation of motion for a rotating system can be expressed in the following manner:

$$T_e = Jeq\frac{d\omega_m}{dt} + B\omega + TL \tag{1.18}$$

Where T_e is the electromagnetic torque for the motor. The illustrated graph, labeled as Figure 1.8, depicts the intended operation of the motor in terms of driving the load, as determined by the aforementioned equations.

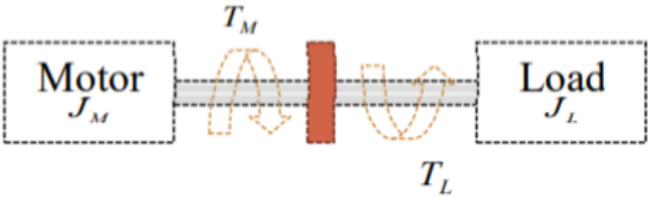

FIGURE 1.8: Mechanical drive of the motor system

1.4 Supply of The Switched Reluctance Motor

1.4.1 Energization of the phase of SRM

The voltage source switched reluctance motor (SRM) drive employs a voltage source supply and a hysteresis controller to achieve alignment between actual and desired currents. It allows for different current waveforms by applying a constant amplitude voltage generator across phases at specific rotor positions. Operating modes A and B exist within the energizing interval, regulating phase current based on the relationship between back electromotive force (emf) and source voltage. The de-energizing interval involves current dissipation without applied voltage. [10]

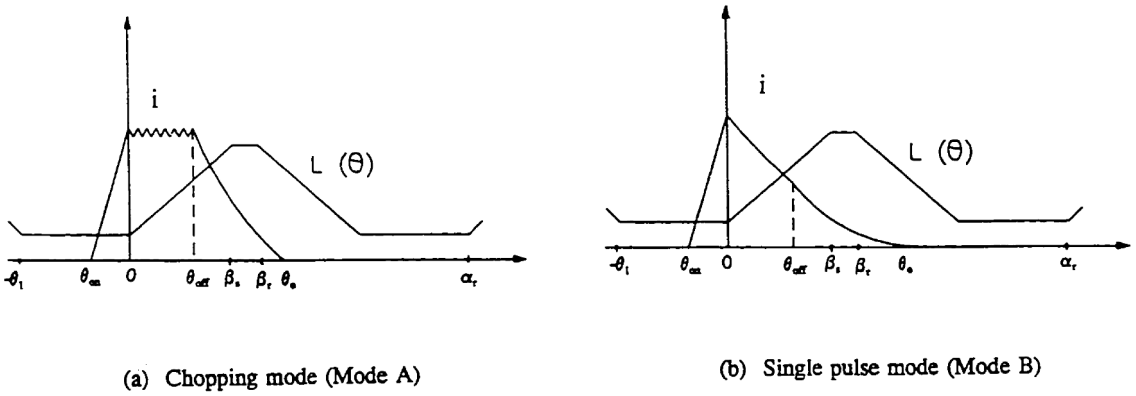

FIGURE 1.9: Typical diagram of the phase current for a VSSRM drive

1.4.2 Asymmetric Half-Bridge Converter

A static converter is necessary to ensure the correct phase excitation and uninterrupted functioning of a (SRM). Among the various topologies available, the asymmetric half-bridge

(AHB) converter is widely employed. This converter topology, depicted in Figure 1.10, enables independent control of each phase of the machine. For each phase, two switches and two diodes are utilized. An advantageous feature of this converter is its versatility, allowing it to drive the machine as a motor or generator with minimal physical modifications.

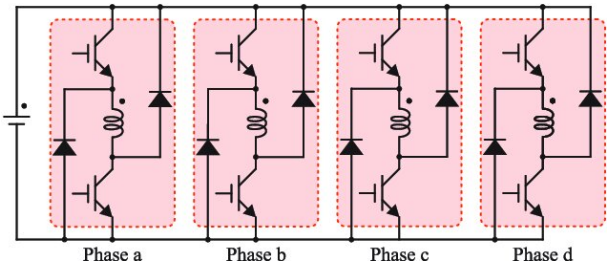

FIGURE 1.10: Four-phase asymmetric half-bridge converter

In the analysis of the AHB converter, each phase is excited individually without overlapping, allowing for separate examination of the switching states, as illustrated in Figure 1.10. The initial switching state occurs when both switches are closed and both diodes are blocked, as depicted in Figure 1.11(a).

During this state, the phase experiences the application of the DC-link voltage, leading to an increase in current while the switches remain closed, representing the magnetization process. Subsequently, when the switches are opened, the energy stored in the winding causes the diodes to become forward biased, enabling the flow of current through a new pathway. This initiates the second switching state of the converter, as presented in Figure 1.11(b).

In the second state, a negative DC-link voltage is applied to the phase, causing a decrease in phase current and demagnetization of the winding. The diodes remain conducting until the switches are closed again or the phase current reaches zero. Additionally, a third switching state can be employed, where only one switch is closed while the other is opened, as illustrated in Figure 1.11(c). This state, referred to as freewheeling, allows current to flow solely through the phase, a switch, and a diode, with zero voltage being applied to the winding [12].

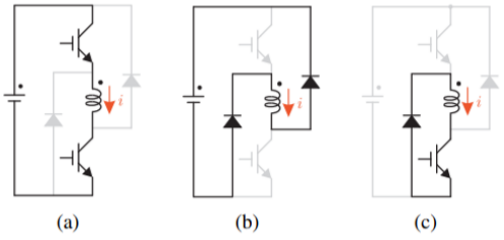

FIGURE 1.11: Asymmetric half-bridge converter switching states. (a) Magnetization. (b)Demagnetization. (c) Freewheeling.

1.5 Simulation of SRM with Current Loop Control

In this section, we will conduct a simulation of the Switched Reluctance Motor (SRM) using Simulink-Matlab. The focus will be on implementing a current loop control, without incorporating any additional control techniques. This simulation aims to evaluate the performance of the SRM under these conditions.

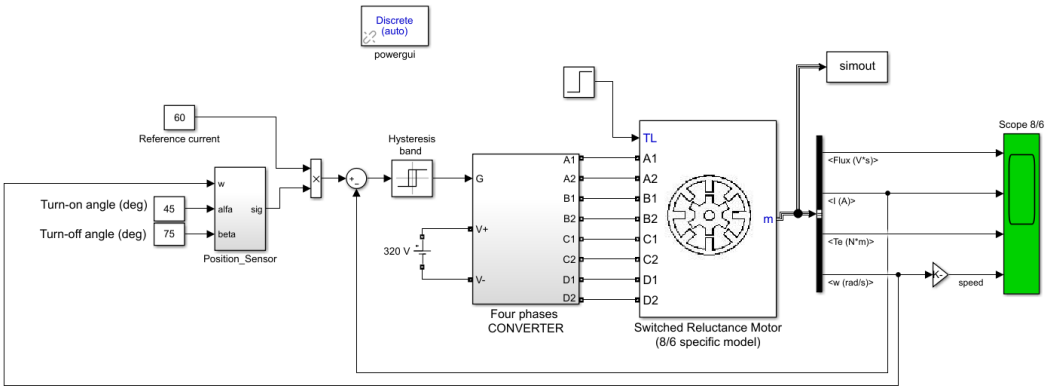

FIGURE 1.12: Block diagram of current loop control of SRM

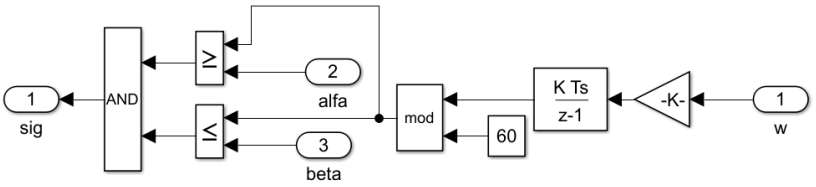

FIGURE 1.13: Position Sensor

1.5.1 Simulation Results

In this section, we initiated the simulation of the Switched Reluctance Motor (SRM) without any external load. Subsequently, at t=0.25s, we introduced a load of 6 N.m.

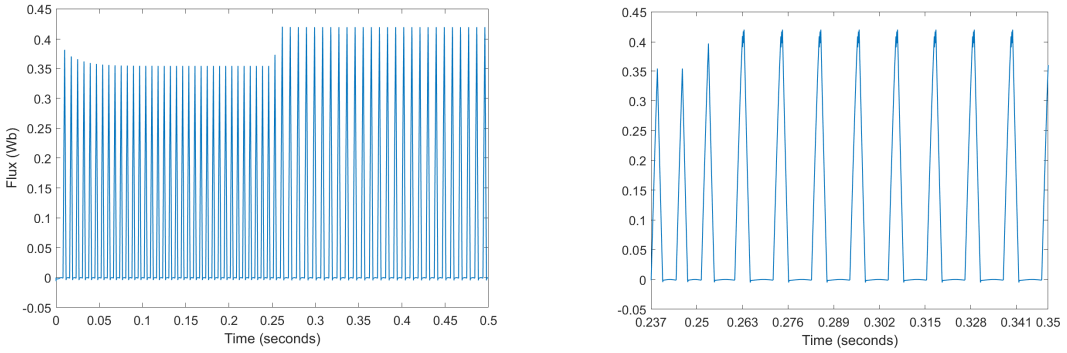

FIGURE 1.14: One phase flux ripples

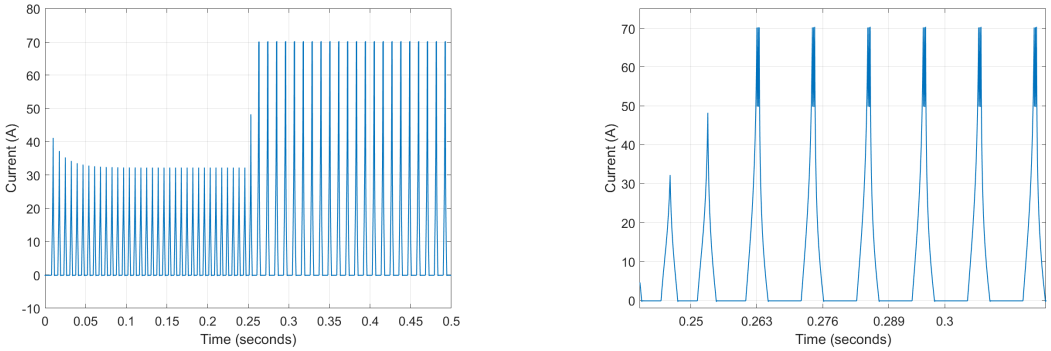

FIGURE 1.15: Output current ripple of one phase

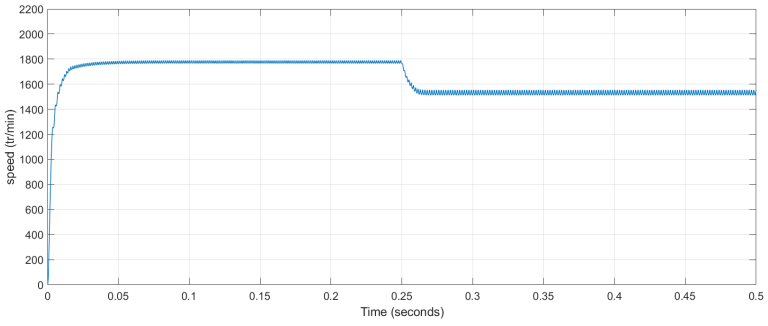

FIGURE 1.16: Motor speed with load

As shown in Figure 1.16, the transitional phase lasts approximately 0.025 seconds, after which the system reaches a stable state with a speed of approximately 1800 revolutions per minute (rpm). However, when a load is introduced at 0.25 seconds, the speed decreases to around 1500 rpm. It becomes evident that there is a significant speed fluctuation, and due to the absence of a regulator, the speed remains reduced.

Once the load is introduced in Figure 1.15, the current of approximately 70 A is achieved, resulting in an increase in current ripple and subsequently leading to an increase in torque ripple. This also applies to the flux, which reaches approximately 0.42 Wb.

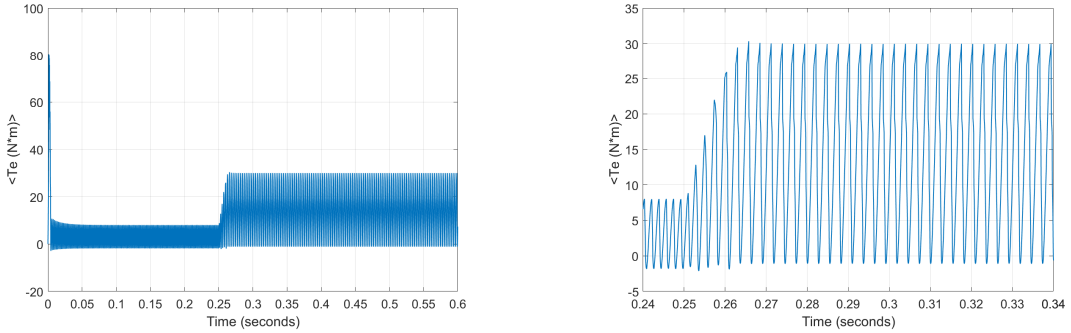

FIGURE 1.17: Torque ripple under load

During the transitional phase showed in Figure 1.17, the torque experiences periodic fluctuations, ranging from 0 up to approximately 80N.m. This transitional regime persists for approximately 0.02s before transitioning into a stable phase. From 0.02s to 0.25s, the torque enters a permanent regime, stabilizing at around 8.5N.m. Furthermore, when a load of 6N.m is applied to the motor, the torque further increases to approximately 30.m. Torque ripple calculation is given by:

$$T_{\text{ripple}} = \left(\frac{T_{\text{max}} - T_{\text{min}}}{T_{\text{mid}}} \right) \times 100 \tag{1.19}$$

$$T_{\text{ripple}} = \frac{T_{\text{max}} - T_{\text{min}}}{T_{\text{mid}}} = 1.15 \times 100 = 115\% \tag{1.20}$$

The depicted machine exhibits significant torque fluctuations, rendering it unsuitable for many applications without the implementation of a control technique aimed at mitigating this problem.

1.6 Conclusion

In this chapter, a thorough examination of the current state of technology was conducted, focusing on the structural and operational aspects of SRMs. The advantages and disadvantages of SRMs were discussed, with one notable drawback being the presence of high torque fluctuation, also known as ripples.

The next chapter will deal with the conventional DTC applied to SRM.

Chapter 2

Direct Torque Control for SRM Using PI Controller

Introduction

The 8/6 4-phase Switched Reluctance Motor (SRM) presents several key issues. Firstly, its non-sinusoidal excitation defies conventional rotating field theory. Secondly, the motor displays highly nonlinear behavior. Thirdly, challenges arise from the interaction between phases during current commutation. Lastly, performing the 4-phase vector transformation poses a difficulty. Additionally, variations and drift in parameters can cause significant deviations in the phase inductance profile compared to the original design data [13].

The direct torque control (DTC) technique employed in the variable reluctance machine involves directly determining the sequence of commands applied to the power converter switches. This approach typically relies on hysteresis comparators, which play a crucial role in regulating the magnitudes of the stator flux and electromagnetic torque. Alternatively, the torque can also be estimated directly by considering the phase currents and rotor position of the machine.

Within the direct torque control methodology, the designated torque reference is compared with the real or estimated torque of the machine. This evaluation enables the determination of the sign of the torque control error. Based on the rotor's position, a specific phase is chosen and activated to either enhance or diminish the machine's torque, aiming to attain the targeted reference torque. This selection process relies on a switching table derived from qualitative rules governing torque behavior, and it forms the central component of the control algorithm [14].

This chapter focuses on the development of a Direct Torque Control (DTC) scheme specifically designed for an 8/6, 4-phase switched reluctance motor.

2.1 Direct Torque Control

2.1.1 Bases of DTC Control

The primary objective of implementing Direct Torque Control (DTC) is to achieve precise regulation of the stator flux and electromagnetic torque. This technique relies on acquiring knowledge of the currents (I_s) and voltages (V_s) of the stator, and optionally the rotor speed (ω_r) for regulation purposes.

During steady-state operation, the stator flux can be readily estimated based on I_s, Vs, and the stator speed (ω_s). The calculation of flux and torque values does not require a complex feedback loop and is independent of the rotor parameters.

Unlike Field-Oriented Control (FOC), where current regulators are employed, DTC directly controls the switches, leading to significantly enhanced performance and offering a notable advantage [15].

2.1.1.1 Stator flux control principle

In the given equation:

$$v_s = R_s I_s + \frac{d\varphi_s}{dt} \tag{2.1}$$

The stator voltage v_s is related to the stator current I_s and the rate of change of stator flux φ_s with respect to time. So,

$$\varphi_s(t) = \int (v_s - R_s I_s) dt \tag{2.2}$$

Within a periodic control interval $[0, T_{\text{sample}}]$, corresponding to a sampling period of T_{sample}, the control of the inverter switches is fixed. It is assumed that the stator resistance remains constant, and for simplicity, we disregard the stator resistance compared to the stator voltage. Hence, we can approximate $\varphi_s(t)$ as:

$$\varphi_s(t) \approx \varphi_{s0} + v_s Te \tag{2.3}$$

where φ_{s0} represents the instantaneous flux vector at time $t = 0$.

Additionally, during a T_{sample} sampling period, the voltage applied to the motor remains constant. Consequently, we can express:

$$\varphi_s(k+1) \approx \varphi_s(k) + v_s T_{\text{samp}} \tag{2.4}$$

This relationship yields:

$$\Delta\varphi_s \approx v_s T_{sample} \tag{2.5}$$

Where:

- $\varphi_s(k)$ is the stator flux vector at the current sampling step.
- $\varphi_s(k+1)$ is the flux vector at the following sampling step.
- $\Delta\varphi_s$ represents the variation of the stator flux vector.
- T_{sample} denotes the sampling period.

It is important to note that $\Delta\varphi_s$ is proportional to the magnitude of the voltage vector applied to the stator. The evolution of the stator flux vector is depicted in the accompanying figure [16].

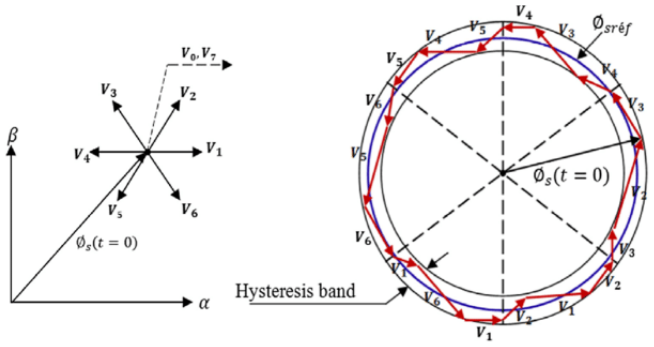

FIGURE 2.1: Stator flux vector trajectory.

2.1.1.2 Principle of electromagnetic torque control

The magnitude of the electromagnetic torque is directly related to the cross product of the stator and rotor flux vectors. This relationship can be expressed by the following equation:

$$T_e = k(\varphi_s \times \varphi_r) = k\,|\varphi_s|\,|\varphi_r|\sin(\gamma) \tag{2.6}$$

Where:

- K is Constant relies on the machine.
- φ_s represents the stator flux vector.
- φ_r indicates the rotor flux vector brought back to the stator.
- γ Refers to the angle formed by the stator and rotor flux vectors.

Based on this equation, the magnitude of the torque relies on the size of the two vectors (φ_s) and (φ_r), as well as their spatial arrangement. In other words, the amplitude of the vectors and their positional relationship are determining factors for the torque.

2.1.1.3 Estimation of flux

The estimation of the flux can be derived by analyzing the recorded measurements of the stator current and voltage in the machine [17]. From the equation:

$$\varphi_s(t) = \int (v_s - R_s I_s) dt \tag{2.7}$$

We obtain the components α and β of the vector φ_s

$$\begin{cases} \varphi_{s\alpha}(t) = \int_0^t (v_{s\alpha} - R_s i_{s\alpha}) dt \\ \varphi_{s\beta}(t) = \int_0^t (v_{s\beta} - R_s i_{s\beta}) dt \end{cases} \tag{2.8}$$

One way to express the estimator in discrete form is by defining it for a specific Tech sampling period using the following formulation:

$$\begin{cases} \varphi_{s\alpha}(k) = \varphi_{s\alpha}(k-1) + [v_{s\alpha}(k-1) - R_s i_{s\alpha}(k-1)] T_{\text{sample}} \\ \varphi_{s\beta}(k) = \varphi_{s\beta}(k-1) + [v_{s\beta}(k-1) - R_s i_{s\beta}(k-1)] T_{\text{sample}} \end{cases} \tag{2.9}$$

The flux modulus and its phase are obtained from the equations of the following system:

$$\varphi_s = \sqrt{\left(\varphi_\alpha^2 + \varphi_\beta^2\right)}, \quad \theta = \arctan\left(\frac{\varphi_\beta}{\varphi_\alpha}\right) \tag{2.10}$$

The variation in the input of the flux hysteresis controller can be expressed as:

$$\Delta\varphi_s = \varphi_{s_{\text{ref}}} - \varphi_s \tag{2.11}$$

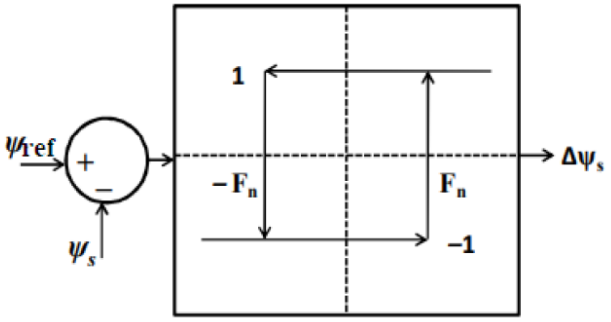

FIGURE 2.2: Two-level hysteresis controller for controlling the flux error.

Figure 2.2 displays the hysteresis controller, which operates at two levels, designed to regulate the flux error. The flux hysteresis loop controller offers a dual digital output, as illustrated in Table 2.1.

TABLE 2.1: Switching Logic for Flux error

state	Flux hysteresis
$\phi_{\text{stator}} - \varphi_{\text{s}} > \Delta\varphi_{\text{s}}$	$1 \uparrow$
$\varphi_{\text{stator}} - \varphi_{\text{s}} < \Delta\varphi_{\text{s}}$	$-1 \downarrow$

2.1.1.4 Estimation of the electromagnetic torque

Once the two components of the flux are acquired, it becomes possible to directly ascertain the torque value. The desired expression can be obtained using the formula provided in reference [18].

$$T_{em} = p(\varphi_{s\alpha} i_{s\beta} - \varphi_{s\beta} i_{s\alpha}) \tag{2.12}$$

In this particular instance, the loop comprises a three-tier hysteresis controller designed to regulate the torque error. The torque error is generated by the disparity between the reference torque and the estimated torque. The control mechanism for the torque hysteresis loop involves three digital output levels, as depicted in Figure 2.3. The corresponding relationships are detailed in Table 2.2. Specifically, when the torque hysteresis band is Tn=1, the torque is increased; when Tn=0, there is no need for any adjustment; and when Tn= –1, the torque is decreased.

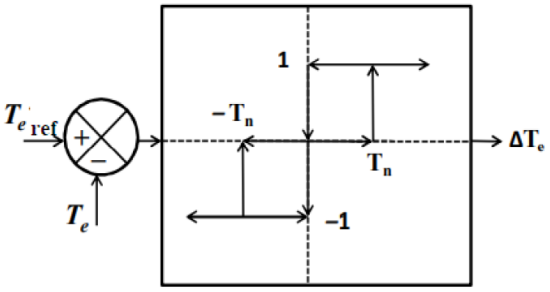

FIGURE 2.3: Three-level Hysteresis Controller for Control of Torque Error

TABLE 2.2: Switching Logic for Torque Error

state	Torque hysteresis
$T_{eref} - Te > \Delta Te$	$1 \uparrow$
$-\Delta T_e < T_{eref} - T_e < \Delta T_e$	0
$T_{eref} - Te < -\Delta Te$	$-1 \downarrow$

2.1.2 Direct Torque Control Applied on SRM 8/6

2.1.2.1 Principle of DTC Applied on SRM 8/6

The equation representing the the instantaneous torque generation in a phase of an SR motor can be formulated as follows:

$$T = i\frac{\partial\varphi(\theta, i)}{\partial\theta} - \frac{\partial W_f}{\partial\theta} \tag{2.13}$$

Where : W_f is the field energy.
The equation for torque production can be derived by employing an approximation that takes into consideration the rarely employed variant of the conventional torque equation. In the case of saturation in the SR motor, the impact of the second term in Equation (2.13) becomes insignificant. Hence, this approximation yields the following equation for torque production.

$$T \approx i\frac{\partial\varphi(\theta, i)}{\partial\theta} \tag{2.14}$$

In the field of SRM (Switched Reluctance Motors), unipolar drives are commonly utilized, resulting in a consistently positive current flow in each motor phase. Consequently, based on Equation (2.14), the torque's sign is directly linked to the change in the stator flux ($\frac{\partial\varphi}{\partial\theta}$).

To generate a positive torque, the stator flux amplitude must increase relative to the rotor position, while a negative torque is achieved when the change in stator flux diminishes in response to the rotor movement.

We can define a positive value of $\frac{\partial \varphi}{\partial \theta}$ as "flux acceleration," whereas a negative value can be termed "flux deceleration" [19]. As a result, a novel technique for controlling SR motors is introduced as follows [20]:

(i) The stator flux linkage vector of the motor is kept at constant amplitude.
(ii) Torque is controlled by accelerating or decelerating the stator flux vector.

The goal of control technique (i) is accomplished in a manner comparable to the conventional DTC utilized for AC machines. This is done by selecting an appropriate voltage vector in the space. Similar to conventional AC machine DTC, the variation in stator flux corresponds to the direction of the voltage vector, and the magnitude of the voltage along with the duration of its application determines the extent of the flux change.

Likewise, objective (ii) is achieved in a similar manner to conventional AC motor DTC, where the torque is adjusted by accelerating or decelerating the stator flux vector in relation to the rotor movement [20].

Figure 2.4 displays the states of the space voltage vectors. These vectors are defined to be positioned at the center of eight zones, denoted as N = 1, 2, ..., 8. Each zone spans an angle of $\frac{\pi}{4}$ radians.

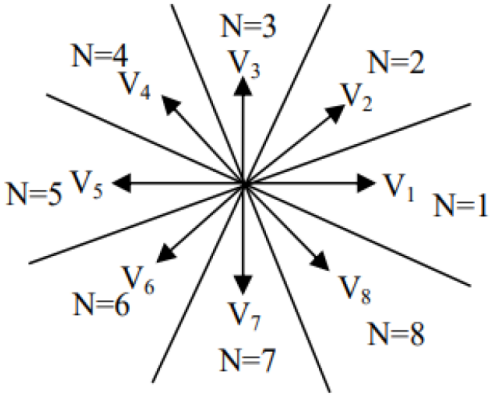

FIGURE 2.4: Definition of SRM motor voltage vectors for DTC

Our 4-phase SRM operates with an asymmetrical converter featuring 8 potential states. To ensure that the stator flux linkage and motor torque remain within hysteresis bands, one of the available states is selected at any given time. Similar to the conventional DTC scheme, when the stator flux linkage falls within the kth zone, the flux magnitude can be increased

by utilizing the switching vectors $V_(k+1)$ and $V_(k-1)$, or decreased by employing $V_(k+2)$ and $V_(k-2)$. Consequently, whenever the stator flux linkage reaches the upper limit of the hysteresis band, voltage vectors are applied to reduce it. These voltage vectors are directed towards the center of the flux vector space, and vice versa.

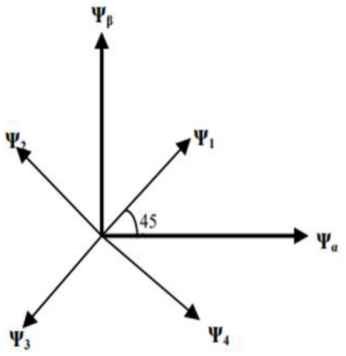

FIGURE 2.5: Definition of 2- axis for motor voltage

As mentioned previously, the manipulation of torque involves adjusting the acceleration or deceleration of the stator flux in relation to the rotor's movement. Consequently, when there is a need for increased torque, voltage vectors are chosen to advance the stator flux linkage in the direction of rotation. These selected vectors are V_{k+1} and V_{k+2}, representing the stator flux linkage in the kth zone. On the other hand, when a reduction in torque is desired, voltage vectors are applied to decelerate the stator flux linkage. These vectors are V_{k1} and V_{k2} in the kth zone. Therefore, a switching table can be established to control the stator flux linkage and motor torque, as illustrated in Table 2.3. In this table, φ_Q=1 and φ_Q=0 indicate an increase and decrease in the flux linkages, respectively, while T_Q=1 and T_Q=0 indicate an increase and decrease in torque, respectively. To consolidate the individual phase flux vectors into a single stator flux linkage vector, the flux vectors for the four-phase SRM are transformed onto a stationary orthogonal two-axis reference frame [19], as depicted in Figure 2.5.

$$\varphi_\alpha \approx \varphi_1 \cos(45) - \varphi_2 \cos(45) - \varphi_3 \cos(45) + \varphi_4 \cos(45) \tag{2.15}$$

$$\varphi_\beta \approx \varphi_1 \sin(45) + \varphi_2 \sin(45) - \varphi_3 \sin(45) - \varphi_4 \sin(45) \tag{2.16}$$

$$\varphi_s = \sqrt{\varphi_\alpha^2 + \varphi_\beta^2}, \quad \theta = \arctan\left(\frac{\varphi_\beta}{\varphi_\alpha}\right) \tag{2.17}$$

The flux vector is represented by φ_s, and its angle is denoted by θ. Meanwhile, the flux-linkages of the four phases are φ_1, φ_2, φ_3, and φ_4.

TABLE 2.3: Switching Table of space voltage vectors

N		1	2	3	4	5	6	7	8
$\varphi_Q = 1$	$T_Q = 1$	V2	V3	V4	V5	V6	V7	V8	V1
$\varphi_Q = 1$	$T_Q = 0$	V7	V8	V1	V2	V3	V4	V5	V6
$\varphi_Q = 0$	$T_Q = 1$	V3	V4	V5	V6	V7	V8	V1	V2
$\varphi_Q = 0$	$T_Q = 0$	V6	V7	V8	V1	V2	V3	V4	V5

2.1.2.2 Speed regulation using PI controller

The P-I controller incorporates both proportional and integral terms in its forward path. By including an integral component, this controller effectively eliminates any steady state error that may arise from a step change. This feature proves highly advantageous in numerous applications. In the case of the SRM drive, the P-I control is implemented while the motor operates within the linear range of its magnetic characteristics. This approach is ideal for evaluating the performance of the control system due to the notable torque ripple and nonlinearity observed in the torque characteristics within this linear region.

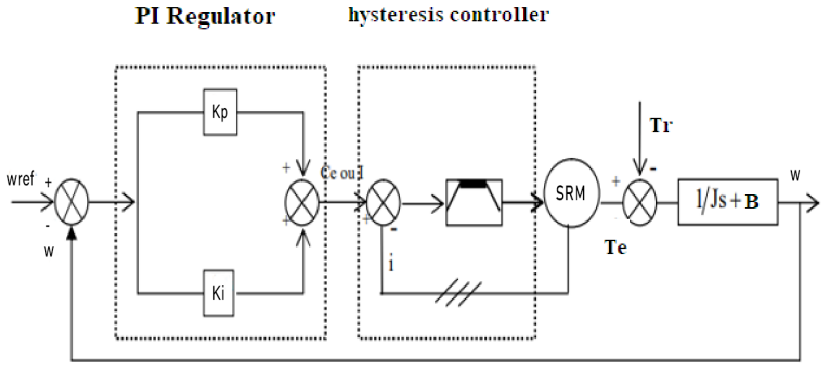

FIGURE 2.6: Speed regulation loop

The adjustment of the electric drive regulator poses a complex challenge due to the multitude of non-linearities inherent in the machine, electronic converter, and controller. Achieving proper controller parameter adjustment becomes difficult due to the persistent non-linearity of the Switched Reluctance Motor (SRM). The power converter exhibits a non-linear transfer characteristic as a result of the dead times imposed by the switching process [21].
When calculating the parameters for the speed PI regulator, it is assumed that the dynamics of the current loops can be disregarded in comparison to the dynamics of the speed loop. This assumption is based on the significantly lower electrical time constant when compared to the mechanical time constant. Consequently, only the mechanical equation of the machine

is taken into consideration and can be expressed in the following form [22]:

$$T_e = J_{eq}\frac{dw_m}{dt} + Bw + T_L \tag{2.18}$$

For the speed controller, the control signal uc represents the total reference torque of the machine T_e^*.

$$T_e^* = k_p(w_{\text{ref}} - w) + k_i \int (w_{\text{ref}} - w)\, dt \tag{2.19}$$

By replacing equation (2.18) in (2.19) with $T_e = T_e^*$, we write:

$$J_{eq}\frac{dw_m}{dt} + Bw + T_L = k_p(w_{ref} - w) + k_i \int (w_{ref} - w)dt \tag{2.20}$$

At any specific time point, denoted as t, it is assumed that the reference speed and load torque remain unchanging, and therefore, their rates of change, or derivatives, are regarded as zero.

$$J_{\text{eq}}\frac{d^2w_m}{dt^2} + (B + k_p)\frac{dw}{dt} + k_i w = k_i w \tag{2.21}$$

We put:

$$\begin{cases} x_1 = \omega \\ x_2 = \frac{d\omega}{dt} \end{cases} \tag{2.22}$$

To provide an overview of the closed loop's state, we can express it as follows:

$$\begin{cases} \dot{x} = Ax + ku \\ y = cx \end{cases} \tag{2.23}$$

With: u = ω^* and y = ω.
Where :

$$A = \begin{bmatrix} 0 & 1 \\ \frac{-k_i}{J} & -\frac{B+k_i}{J} \end{bmatrix}, \quad k = \begin{bmatrix} 0 \\ \frac{k_i}{J} \end{bmatrix}, \quad C = \begin{bmatrix} 1 & 0 \end{bmatrix}$$

The relationship between the input of the source and the output of the closed loop system can be described by the following transfer function equation:

$$G(s) = \frac{\frac{k_i}{J}}{s^2 + \left(\frac{B+k_p}{J}\right)s + \frac{k_i}{J}} \tag{2.24}$$

The denominator of a typical second-order system can be employed to depict the denominator of the transfer function in a closed-loop configuration.

$$s^2 + \left(\frac{B}{J} + \frac{k_p}{J}\right)s + \frac{k_i}{J} = s^2 + 2w_n\xi s + w_n^2 \tag{2.25}$$

By identification, the PI speed regulator parameters are given by:

$$\begin{cases} k_p = 2Jw_n\xi - B \\ k_i = Jw_n^2 \end{cases} \tag{2.26}$$

When the damping coefficient is assigned a value of one, the dynamics of the speed response are governed by the relevant natural frequency, ω_n, and the damping coefficient, ξ, of the looped system.
Upon replacing the PI controller in our system, the resulting control behavior is demonstrated as:

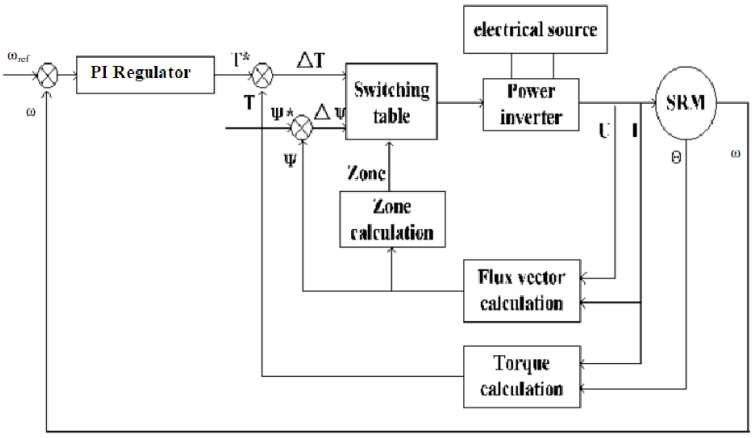

FIGURE 2.7: DTC with PI speed regulator for SRM

2.2 Simulation and Results

To showcase the effectiveness of the conventional Direct Torque Control (DTC) with a PI regulator for SRM, a comprehensive numerical simulation was conducted across various scenarios.

2.2.1 Block diagram of classic DTC

The MATLAB/SIMULINK software is utilized to model and simulate the DTC of a 4-phase 8/6 SRM. Within Fig. 2.8, a simulation model featuring a PI controller is presented, which encompasses an asymmetrical 4-phase converter alongside the 8/6 SRM.

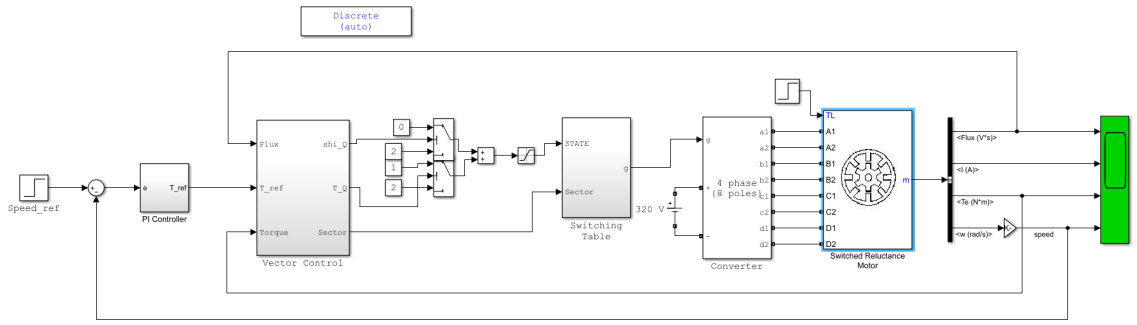

FIGURE 2.8: Block diagram of DTC with PI regulator of SRM

The calculation of flux in each phase is performed by the flux linkage computation block. The $\alpha\beta$ block receives the output of the flux linkage computation block, converting the flux values from 4 phases to 2 phases.

The magnitude φ_s and angle θ of the flux vector are determined through the flux vector calculation block. Subsequently, the flux vector magnitude φ_s and the motor torque T, obtained from the motor, are supplied to the flux and torque hysteresis blocks. Along with the reference values of flux and torque, these inputs are utilized in the flux and torque hysteresis blocks.

The hysteresis blocks control the generation or reduction of flux (φ_Q) and torque (T_Q) based on the current magnitudes of flux and torque within specific ranges. The switching table and asymmetrical converter then apply the appropriate voltage vectors to the windings of the switched reluctance motor (SRM).

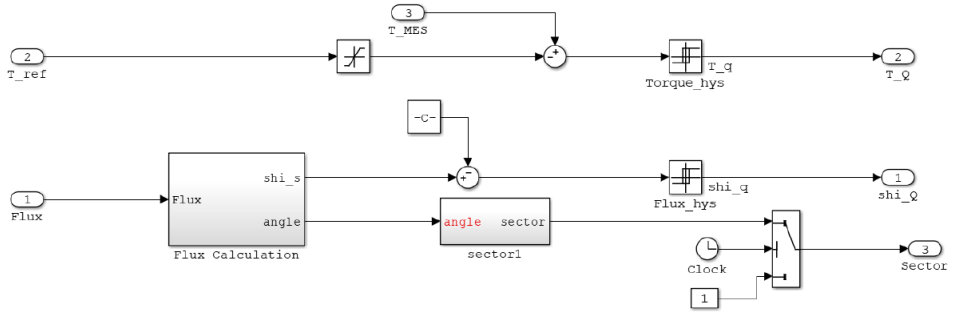

FIGURE 2.9: Flux and torque hysteresis controller plus sector determination

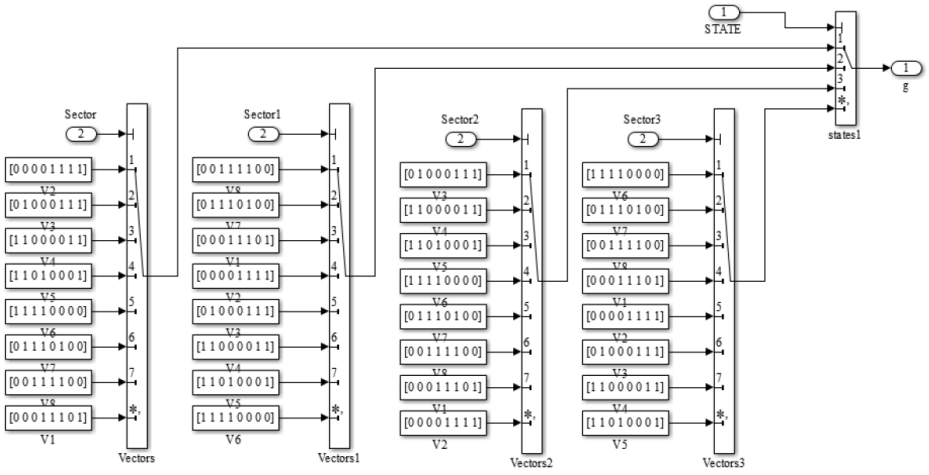

FIGURE 2.10: Switching table

The simulation test involves utilizing a motor reference flux of 0.264 Wb and applying a load torque of 6 Nm at 0.25s. For the flux linkage and torque, hysteresis bands of 0.02Wb and 0.2 Nm respectively were established. Various simulation results of DTC implemented on SRM are depicted in the accompanying figures.

The outcome of the simulation is displayed in Figure 2.11. The simulation lasted for a period of 0.5 seconds. The subsequent section showcases the specific outcomes of each system output, accompanied by a comprehensive discussion.

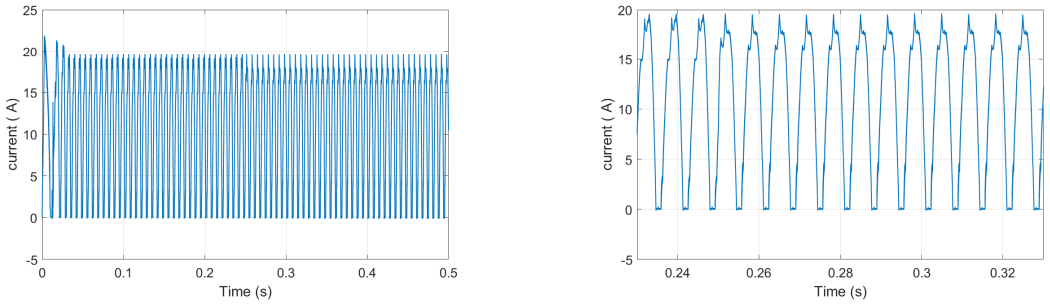

FIGURE 2.11: Output current ripple of one phase

The given scenario, the current in a single phase initially reaches approximately 22A within a transit time of approximately 0.02 seconds. After this, it stabilizes at 19.8A. When a torque of 6N.m is applied at 0.25 seconds, the current stays at 19.8A. Nevertheless, the application of the load torque leads to an increase in current ripples.

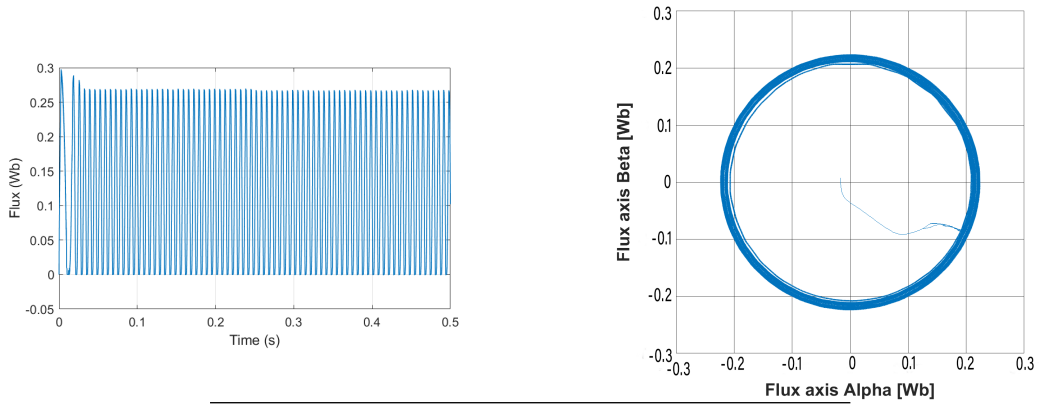

FIGURE 2.12: One phase flux linkage ripple and the total stator flux vector

Figure 2.12 presents the outcome of the control of stator flux linkage, showcasing separate plots that illustrate the amplitude and trajectory of the overall stator flux vector. Upon examining the diagram, it is evident that the amplitude of the stator flux vector remains relatively consistent, measuring approximately 0.26Wb, which serves as the reference flux value.

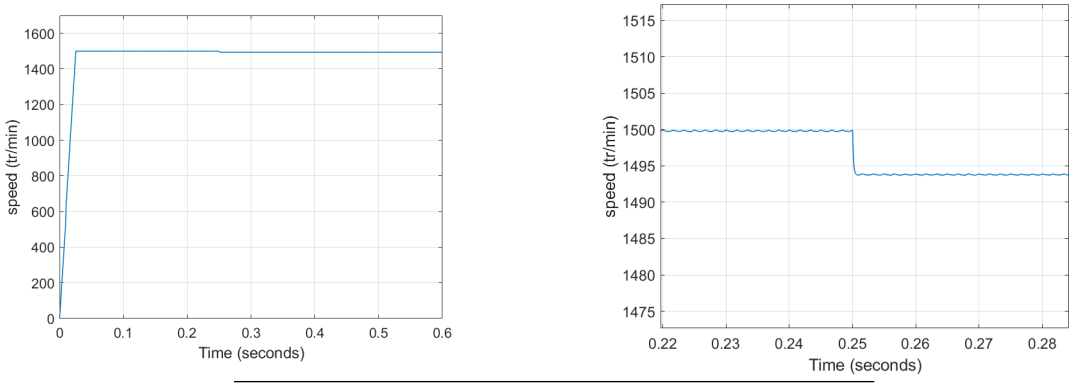

FIGURE 2.13: Speed of the motor with zoom at the time of loading the motor

The simulation results demonstrated in Figure 2.13 show that the actual speed closely follows the reference speed within approximately 0.05 seconds. To achieve this, a PI controller is employed, enabling the actual speed to track the reference speed. At 0.25 seconds, when a load torque of 6 N.m is introduced, the actual speed only exhibits a slight deviation from the reference speed.

Figure 2.14 demonstrates that the torque is directly proportional to the square of the current, irrespective of its direction. However, the torque is affected by the derivative of L with respect to θ ($\frac{dL}{d\theta}$). If this derivative is positive, the torque is positive, and if it is negative, the torque becomes negative. Notably, the torque oscillates within a range of 1.1 N.m to -0.2 N.m. Additionally, at 0.25s, a load torque of 6 N.m is applied, resulting in an increase in torque from approximately 7.1 N.m to 5.55 N.m.

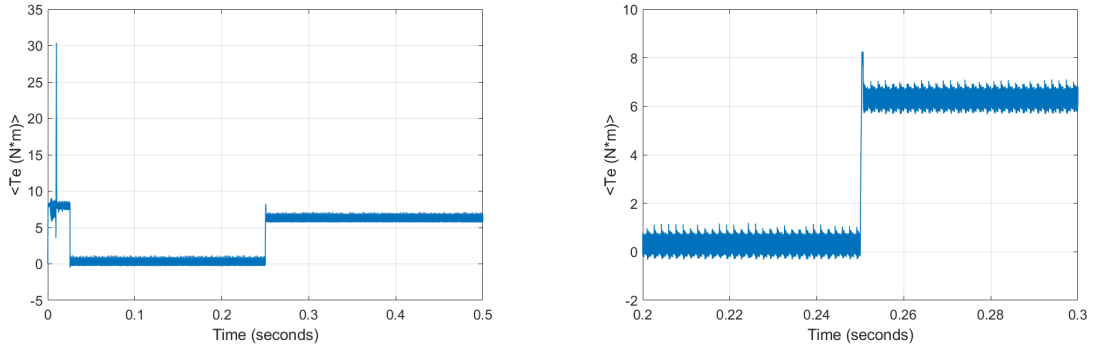

FIGURE 2.14: Torque ripples

By employing the direct torque control technique, we have significantly reduced the noise and vibration compared to when only the current loop control was utilized.

$$T_{ripple}] = \frac{T_{max} - T_{min}}{T_{mid}} * 100 = 25\% \tag{2.27}$$

2.3 Conclusion

This chapter provides a comprehensive explanation of the Direct Torque Control (DTC) applied to a 4-phase 8/6 Switched Reluctance Motor (SRM). The direct control of torque is achieved by manipulating the flux linkage magnitude and the speed change of the stator flux vector. To assess the performance of the DTC-SRM drive, a suitable combination of 8 space voltage vectors is selected. It is observed that the torque ripple amounts to 12.68%. Although the performance of the Proportional-Integral (PI) regulator is acceptable, there is room for improvement in terms of dynamic response and robustness. The PI regulator's dependence on parameters for gain calculation makes it vulnerable to deviations in case of parametric variations, resulting in an inadequate response.

Considering the aforementioned circumstances, the next chapter will introduce a couple of robust control techniques approach for DTC, such as sliding mode control, Twisting control, and Super Twisting control to be implemented on SRMs.

Chapter 3

High Order Sliding Mode Control of SRM

Introduction

Variable Structure Control (VSC) with Sliding Mode Control (SMC) was initially developed in the 1950s by Emelyanov and his colleagues in the Soviet Union. It gained recognition as a robust control technique by the 1970s and has since generated significant interest in the control research community.

SMC is a nonlinear control method known for its accuracy, robustness, and ease of implementation. It involves guiding system states to a sliding surface in the state space and maintaining them in close proximity to the surface using a two-part controller design.

SMC offers advantages in tailoring system behavior and handling uncertainties. However, conventional sliding-mode control suffers from chattering, which can be mitigated using techniques like Higher Order Sliding Mode.

In this context, the chapter focuses on designing an SMC for a Switched Reluctance Motor (SRM) and proposes the Twisting and Super-Twisting algorithm controllers to reduce chattering and regulate the speed of the SRM.
Simulation results will be presented to validate the effectiveness of this approach.

3.1 Sliding mode control

The SMC method is a popular approach in the field of automatic control due to its ability to adapt to uncertainties, its quick response, and its straightforward implementation in both software and hardware [26]. The fundamental principle of SMC involves guiding the system

trajectory along a switching surface using a specific control law. This process can be divided into two distinct phases: the reaching phase, where the state trajectory is directed towards the surface S= 0 and eventually reaches it within a finite period of time, followed by the sliding phase, during which the trajectory glides along the switching surface towards an equilibrium point [27]. This is illustrated in Figure 3.1.

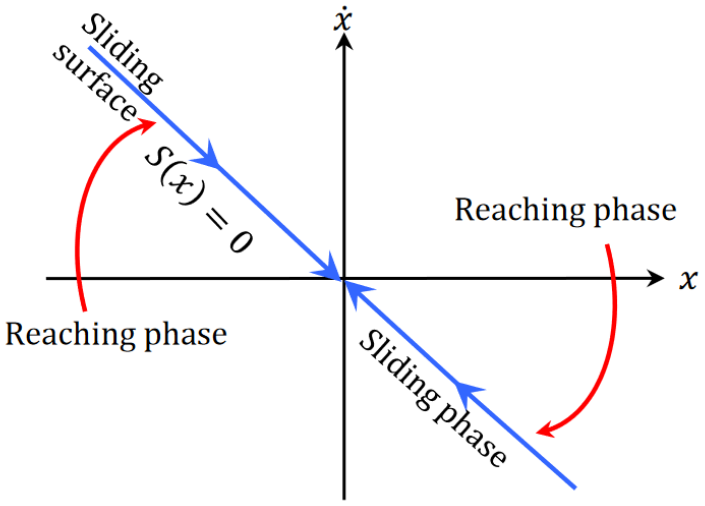

FIGURE 3.1: Sliding mode principle of state trajectory.

3.1.1 Sliding surface choice

Consider the given differential equation that characterizes the system, with f and g denoting nonlinear functions. It is assumed that g possesses an invertible property [27].

$$\dot{x} = f(x,t) + g(x,t)u \tag{3.1}$$

u: the system entry.
x: system state.
Let xd be the desired set point and e the following error defined by:

$$e = x - x_d \tag{3.2}$$

The sliding surface's general formula is determined based on the system's order as outlined below:

$$s(x) = \left(\frac{d}{dt} + \gamma\right)^{n-1} e(x) \tag{3.3}$$

Where:

- s : the sliding surface.
- γ : is a positive constant.
- e : refers to the system error.
- n : the system relative order

3.1.2 Existence conditions of sliding mode

The presence of the sliding mode is required at every point on the surface S = 0. In order to ensure that the system remains in the sliding mode even after the reaching phase, certain conditions need to be fulfilled, which are:

$$\begin{cases} \lim_{S\to 0^-} \dot{S} < 0 \\ \lim_{S\to 0^+} \dot{S} > 0 \end{cases} \tag{3.4}$$

If S has a positive value, its derivative should have a negative value, whereas if S has a negative value, its derivative should have a positive value. This concept can be expressed in a more concise form as:

$$S\dot{S} < 0 \tag{3.5}$$

Given that the problem of existence bears resemblance to a broader stability problem, it can be concisely expressed using Lyapunov's theory as follows [27].

$$V = \frac{1}{2}S^2 \tag{3.6}$$

The objective is to establish a governing principle that ensures $\dot{V} < 0$, aiming to guide the system's states towards the sliding-mode surface.

$$\dot{V} = S\dot{S} < 0 \tag{3.7}$$

When $S \neq 0$, $\dot{V}$ is characterized by negativity. Consequently, in order to achieve convergence within a finite timeframe, it is necessary for the condition (3.5) to be satisfied, as it guarantees asymptotic convergence towards the sliding surface.

3.1.3 Control design

Literature presents several techniques for control design, including relay control, equivalent control scheme, and linear feedback with switched gains. Among these methods, the equivalent control structure is widely employed in electrical machine control (see Fig. 3.2). This preference stems from its compatibility with the power electronics converters, making it a more suitable option compared to relay control [28].

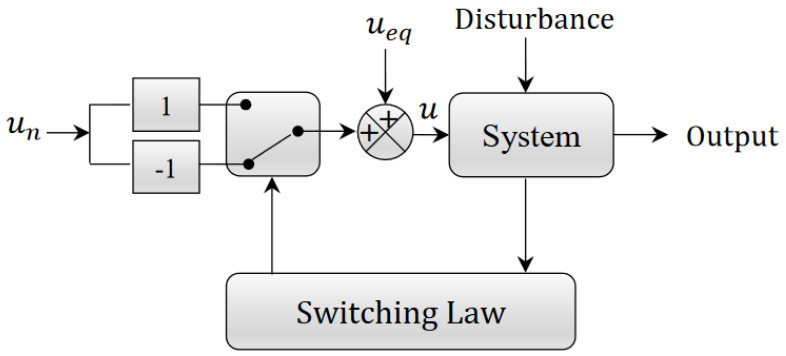

FIGURE 3.2: Equivalent control structure.

The process of designing sliding mode control involves two main components. Firstly, an additional control term called the equivalent control (u_{eq}) is combined with the discontinuous control (u_n). This combination is crucial for ensuring that the state trajectory reaches and remains on the switching surface.
The control law is mathematically represented by the following expression:

$$u = u_{eq} + u_n \tag{3.8}$$

By considering the following state system:

$$\dot{X} = A(x) + B(x)u \tag{3.9}$$

To determine the corresponding control, it is essential to acknowledge that the condition S=0 is indispensable for the state trajectory to remain on the switching surface S=0 [39].
The time derivative of the sliding surface is given as:

$$\dot{S} = \frac{\partial S}{\partial t} = \frac{\partial S}{\partial x}\frac{\partial x}{\partial t} \tag{3.10}$$

By substituting (3.8) and (3.10) into Eq (3.9):

$$\dot{S} = \frac{\partial S}{\partial x}A(x) + \frac{\partial S}{\partial x}B(x)u_{eq} + \frac{\partial S}{\partial x}B(x)u_n \tag{3.11}$$

The equivalent control is determined throughout the sliding phase and the steady state where $S = \dot{S} = 0$ and $u_n = 0$ [28].

$$u_{eq} = -\left(\frac{\partial S}{\partial x}B(x)\right)^{-1}\frac{\partial S}{\partial x}A(x) \tag{3.12}$$

The existence of an inverse matrix is a necessary, which means the next condition (3.13):

$$\frac{\partial S}{\partial x}B(x) \neq 0 \tag{3.13}$$

After inserting Equation (3.12) into Equation (3.11), the resulting expression for the sliding surface is as follows:

$$\dot{S} = \frac{\partial S}{\partial x}B(x)u_n \tag{3.14}$$

The determination of the discontinuous control variable u_n occurs during the convergence phase, and it is essential to ensure the condition of finite time convergence, denoted as $S\dot{S} < 0$. This condition is defined as follows:

$$S\dot{S} = S\frac{\partial S}{\partial x}B(x)u_n < 0 \tag{3.15}$$

To meet this requirement, the value of u_n must have the opposite sign of $S\frac{\partial S}{\partial x}B(x)$. The concept of discontinuous control entails a switching term created by multiplying the relay function $sign(S)$ by a constant coefficient K. The relay function is defined by:

$$sign(S) = \begin{cases} +1 & \text{if } S \geq 0 \\ -1 & \text{if } S < 0 \end{cases} \tag{3.16}$$

$$u_n = -Ksign(S) \tag{3.17}$$

To ensure the convergence condition, it is necessary for the coefficient K to be positive. In our specific use cases, we will substitute the expression "$sign(S)$" with the sigmoid function "$sigm(S)$" to mitigate the impact of chattering.

$$sigm(S) = \left(\frac{2}{1 - e^{qS}}\right) - 1 \tag{3.18}$$

The value of q is a small, positive constant that modifies the slope of the sigmoid function.

3.1.4 Chattering phenomenon

In real-world implementations of sliding mode control, engineers may encounter an undesirable occurrence referred to as "chattering" (illustrated in Figure 3.3). Chattering is a detrimental phenomenon that manifests as oscillations with finite frequency and amplitude.

It poses several negative consequences, such as diminished control precision, increased wear on mechanical components, and elevated heat dissipation in power circuits. The primary factors contributing to this phenomenon are restrictions imposed by the actuator and delays in the control-level switching processes [29].

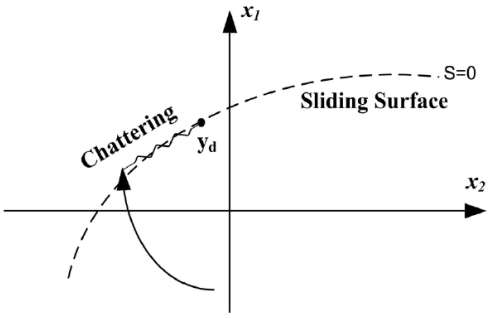

FIGURE 3.3: The chattering phenomenon

3.1.5 Solutions to reduce the Chattering phenomenon

Numerous approaches have been suggested to address and potentially resolve this occurrence, aiming to minimize or eradicate its impact. These proposed solutions encompass a range of strategies, including the boundary layer solution, fuzzy sliding mode, higher order sliding mode, and approach law [30].

3.1.5.1 Changing the switching function

A commonly employed approach to address this issue involves substituting the traditional sign(x) function with smoother switching functions. Notably, the saturation function (sat(x)) [30] and the sigmoid function (sigm(x)) [31] are often utilized for this purpose, as illustrated in Figure 3.4.

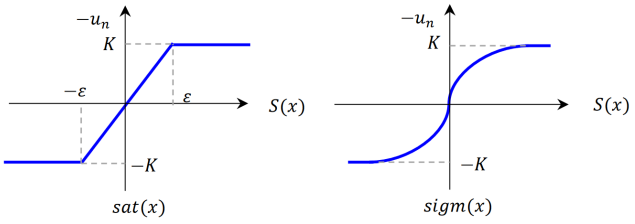

FIGURE 3.4: Saturation and sigmoid functions.

The shown functions are defined by:

$$sat(x) = \begin{cases} 1 \quad if \quad x > \epsilon \\ \frac{x}{\epsilon} \quad if \quad |x| \leq \epsilon \\ -1 \quad if \quad x < -\epsilon \end{cases} \tag{3.19}$$

$$sigm(x) = \left(\frac{2}{1 + e^{\alpha S}} - 1 \right) \tag{3.20}$$

Where:

- ϵ is a small positive constant representing the width of boundary layer.
- α is a small positive constant which adjusts the sigmoid function slope.

3.1.5.2 Solution by approach laws

A noteworthy approach involves using nonlinear convergence laws to adapt a command component based on the sliding function's variations. This allows for reducing high-frequency switching during steady-state operation without impacting convergence time or tracking error. Gao and Hung proposed two laws to minimize switching, with the first law facilitating quicker reaching of the sliding surface by incorporating a term proportional to the sliding function and alleviating the impact of the discontinuous part sign(s).

$$\dot{s} = -\alpha \cdot sign(s) - Q \cdot s \tag{3.21}$$

The second law of convergence incorporates a fractional exponent that affects the function of s and modifies its sign in the following manner:

$$\dot{s} = \alpha |s| \rho sign(s) \tag{3.22}$$

Where ρ is a real strictly between 0 and 1. It is also demonstrated by Gao and Hung that the law of convergence generates a finite reach time of the sliding surface.

3.1.5.3 Solution by higher order sliding modes controllers

Higher-order sliding modes were introduced as a solution to the problem of chattering in classical sliding mode controls. By incorporating the discontinuous term in one of the higher derivatives of the synthesized command, this approach effectively reduces chattering while preserving the desired properties of finite-time convergence and robustness.

3.2 Second order sliding mode control

Classic sliding modes offer robustness and high precision in control problems under uncertain conditions. However, there are two main limitations that need attention. Firstly, conventional sliding modes require a constraint with a relative degree of 1, meaning that the control variable must appear explicitly in the first derivative of the constraint. This necessitates finding a suitable constraint. Secondly, frequent high-frequency switching of the control signal can lead to practical issues, such as the undesirable chattering effect, especially when the control has physical implications.

To address the objective of keeping the sliding variable (s) at zero with the control appearing only in the second derivative ($\ddot{s}$), a common choice is the constraint function $\sigma = s + \dot{s}$. By utilizing classic sliding mode techniques, the derivative of σ contains the control term, enabling the maintenance of σ at zero and the asymptotic approach of 's' towards zero.

Alternatively, if the control term already appears in the first derivative of (s), conventional sliding modes provide a straightforward solution. However, the chattering effect often renders this solution unacceptable. To mitigate this issue, a possible solution involves considering the control derivative as a new virtual control. By employing a second-order sliding mode technique, precise achievement of the objective within a finite time frame becomes possible using continuous control. Consequently, the chattering effect is expected to be significantly reduced.

3.2.1 Control design

Let us examine a dynamic system that takes the following structure:

$$\dot{x} = f(t, x) + g(t, x)u \tag{3.23}$$

The aim is to achieve a second-order sliding regime in relation to 's' by compelling the system's state trajectories to transition onto the 's_z' set within a finite time and remain within it thereafter [32].

$$\ddot{s} = \{x : s = \dot{s} = 0\} \tag{3.24}$$

The intended outcome is accomplished through the utilization of a directive that operates on the secondary derivative of the shifting parameter. Typically, this secondary derivative can be expressed in the following manner:

$$\ddot{s} = \phi(x, t) + \varnothing(x, t) \cdot u \tag{3.25}$$

To implement second-order sliding mode algorithms effectively, it is imperative to confirm the following assumptions to ensure the attainability of the sliding surface and the stability of the variable $\ddot{s}$:

- the functions (x, t) and ϕ(x, t) are some unknown smooth functions
- Within a specific range of $|s(x,t)| < S_0$, the following inequalities are satisfied, where S_0, C_0, K_m, and K_M are positive constants:
  $|\phi(x,t)| < C_0 \quad \text{and} \quad 0 < K_m \leq \varnothing(x,t) \leq K_M$

The aforementioned assumptions suggest that the second derivative of the switching function remains bounded uniformly within a specific domain (E1) for the given input.
By adhering to the established conditions, it can be stated that any solution pertaining to Equation (3.2) fulfills the subsequent differential inclusion:

$$\ddot{s} \in [-C_0, C_0] + [K_m, K_M] \cdot v \tag{3.26}$$

3.2.2 Examples of second order sliding mode control

Several second-order sliding mode algorithms have been introduced in the literature [33] [34]. Of these algorithms, we would like to mention:

- Twisting algorithm.
- Super Twisting algorithm.
- Control Algorithm with Prescribed Convergence Law.
- Quasi-Continuous Control Algorithm.

3.2.3 Twisting algorithm

The controller mentioned below represents the first-ever second-order sliding mode controller proposed in history. Its definition is presented through the formula [33].

$$u = -\left(r_1 sign(s) + r_2 sign(\dot{s})\right), r_1 > r_2 > 0 \tag{3.27}$$

Provided that the inequalities (3.26) are satisfied, the trajectory of the differential system (3.24) will reach the equilibrium point where s = $\dot{s}$ = 0 within a finite duration, given the

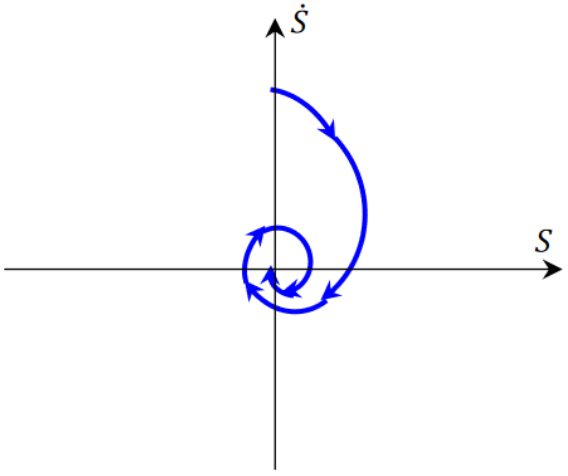

FIGURE 3.5: Twisting controller trajectory

following criteria:

$$\begin{cases} (r_1 + r_2) \cdot K_m - C_0 & > (r_1 + r_2) \cdot K_M + C_0 \\ (r_1 + r_2) \cdot K_m & > C_0 \end{cases} \tag{3.28}$$

The uniformity of this control law is apparent since its formulation is independent of the specific values of s or $\dot{s}$, relying only on their signs, which remain consistent even when multiplied by a positive constant K.

3.2.4 Super Twisting algorithm

The super-twisting algorithm introduced by Levant, offers a solution for nth order sliding mode control algorithms. Unlike its counterparts, this algorithm eliminates the need for information on S, $\dot{S}$, $\ddot{S}$,... ,S^{n-1}, instead focuses only on S. It achieves continuous control without requiring the evaluation of the sign of S. Additionally, the convergence of this algorithm is explained through the rotation around the origin in the phase diagram (S, $\dot{S}$).

The super twisting algorithm possesses an advantage compared to other algorithms as it does not require the time derivatives of the sliding variable. The control law u_{ST} of the super twisting (ST) algorithm consists of two components. The first component, u_1, is a discontinuous term defined by its time derivative $\dot{u_1}$. The second component is determined by the function of the sliding variable, u_2. The definition of the ST control law is as follows:

$$\dot{u_1} = \begin{cases} -u_1 & if \quad |u| > 1 \\ -Ksign(S) & if \quad |u| \leq 1 \end{cases} \tag{3.29}$$

$$u_2 = \begin{cases} -\lambda |S_0|^{\rho} sign(S) & if \quad |S| > S_0 \\ -\lambda |S|^{\rho} sign(S) & if \quad |S| \leq S_0 \end{cases} \tag{3.30}$$

λ and K are positive gains used to adjust the ST controller.

Achieving convergence of the control law can be accomplished by flexibly adjusting these gains [38]. In general, the gain λ significantly influences the system's response, while the gain K impacts the accuracy of the steady state. Levant [37] has proposed certain conditions that ensure finite-time convergence which are:

$$\begin{cases} K > \frac{\psi}{\Gamma_M} \\ \lambda \geq \frac{4\psi\Gamma_M(\beta+\psi)}{\Gamma_m^3(\beta-\psi)} \end{cases} \tag{3.31}$$

The value of φ represents the upper limits of the uncertain function ϕ, while Γ_m and Γ_M indicate the lower and upper limits of the uncertain function γ at the second derivative of the sliding manifold [37].

$$\varphi \geq \phi \quad and \quad \Gamma_M \geq \gamma \geq \Gamma_m \tag{3.32}$$

The level of nonlinearity can be modified by the coefficient ρ, which is restricted to the range of (0 ¡ $\rho \leq 0.5$). Typically, it is set to "0.5" in order to attain the maximum effectiveness of second-order sliding mode control. When the controlled system exhibits linear dependence on the control law, it can be simplified. In this case, ψ, S_0, Γ_m, and Γ_M are treated as fixed positive values, and the ST control law can be expressed as follows:

$$\begin{cases} u_{ST} = -\lambda |S|^{\frac{1}{2}} sign(S) + u_1 \\ \dot{u_1} = -K sign(S) \end{cases} \tag{3.33}$$

3.2.5 Design of sliding mode controllers

3.2.5.1 First order SM-speed controller design

The rotor speed's sliding surface is determined by:

$$\begin{cases} S_{wr} = \omega_r^* - \omega_r \\ \dot{S_{wr}} = \dot{\omega_r^*} - \dot{\omega_r} \end{cases} \tag{3.34}$$

The mechanical equation of induction motor is given as:

$$\dot{\omega_r} = \frac{1}{J}(T_e - T_L) - \frac{B}{J}\omega_r \tag{3.35}$$

The equation for the derivative of the speed surface can be obtained by substituting Equation (3.35) into it, resulting in the following expression:

$$\dot{S_\omega} = \dot{\omega_r} - \frac{1}{J}(T_e - T_L - B\omega) \tag{3.36}$$

By utilizing the principles of sliding mode theory, it is possible to express the concept as follows:

$$T_e = T_{eeq} + T_d \tag{3.37}$$

The equivalent control component is determined when the sliding mode state $\dot{S_\omega}$=0 is reached. Subsequently, the equivalent control can be expressed as follows:

$$T_{eeq} = B\omega + T_L \tag{3.38}$$

The discontinuous part is defined as:

$$T_d = K_{\omega_r} sign(S_{\omega_r}) \tag{3.39}$$

Where K_{ω_r} is a positive gain

3.2.5.2 Twisting SM-speed controller design

For speed regulation we are interested in the dynamics of speed error e, defined as:

$$e(t) = \omega^* - \omega \tag{3.40}$$

where ω^* is the desired speed and is assumed to be a known constant.
By replacing e(t) in Equation (3.3) we get:

$$s(x) = \gamma e(t) + \dot{e}(t) \tag{3.41}$$

Also we have:

$$\begin{cases} \frac{d\theta}{dt} = \omega \\ \dot{\omega_r} = \frac{1}{J}(T_e - T_L - B\omega) \\ \frac{di_{ph}}{dt} = \left(\frac{\partial \varphi_{ph}(\theta, i_{ph})}{\partial i_{ph}}\right)^{-1} (u_{ph} - Ri_{ph} - \omega \frac{\partial \varphi_{ph}(\theta, i_{ph})}{\partial \theta}) \end{cases} \tag{3.42}$$

ph = 1, 2, 3, 4

Where,

$$\dot{e} = \dot{\omega^*} - \dot{\omega} \qquad with \quad \dot{\omega^*} = 0 \tag{3.43}$$

So:

$$\dot{e} = \dot{\omega} = \frac{1}{J}\left[\sum_{ph=1}^{4} T_{ph}(\theta_{ph}, i_{ph}) - B\omega - TL\right] \tag{3.44}$$

For realizing our twisting controller, we have:

$$\dot{s}(x) = \gamma\dot{e} + \ddot{e} \tag{3.45}$$

So we get:

$$\begin{cases} \ddot{w} = \frac{1}{J}\left(\frac{dTe}{dt} - B\frac{dw}{dt} - \frac{dTL}{dt}\right) \\ \ddot{w} = \frac{1}{J}\left(\sum_{ph=1}^{4} \frac{dT_{ph}(\theta,i_{ph})}{dt} - B\dot{w} - \frac{dTL}{dt}\right) \\ \ddot{w} = \frac{1}{J}\left(\sum_{ph=1}^{4} \frac{\partial T_{ph}(\theta,i_{ph})}{\partial i_{ph}}\frac{di_{ph}}{dt} + w\sum_{ph=1}^{4} \frac{\partial T_{ph}(\theta,i_{ph})}{\partial \theta} - B\dot{w} - \frac{dTL}{dt}\right) \end{cases} \tag{3.46}$$

The next step involves substituting the sliding surface in equation (3.27) we get:

$$u = -\left(r_1 \sin(\gamma e + \dot{w}) + r_2 \sin(\gamma\dot{w} + \ddot{e})\right), \quad r_1 > r_2 > 0 \tag{3.47}$$

3.2.5.3 Super Twisting SM-speed controller design

The design of the speed control law for the second order sliding mode will involve combining the equivalent control with the super twisting control law. The approach to designing the super twisting speed controller (STSC) is as follows:

$$\begin{cases} u_{ST} = -\lambda_{wr}|S_{wr}|^{\frac{1}{2}} sign(S_{wr}) + u_1 \\ \dot{u_1} = -K_{wr} sign(S_{wr}) \end{cases} \tag{3.48}$$

λ_{wr} and K_{wr} are the super twisting speed controller gains.
The expression denoting the reference torque produced by the second order sliding mode controller can be stated as follows:

$$T_{eref} = T_{eeq} - u_{ST} \tag{3.49}$$

In order to ensure the stability of speed control, the super twisting control law needs to satisfy the Lyapunov stability condition. The calculation of the derivative of the Lyapunov candidate is as follows:

$$\dot{V} = S_{wr}\dot{S_{wr}} < 0 \tag{3.50}$$

By substituting (3.50) in (3.37) we obtain:

$$\dot{S_{wr}} = -\frac{1}{J}(u_{ST}) = -\frac{1}{J}\left(\lambda_{wr}|S_{wr}|^{\frac{1}{2}} sign(S_{wr}) + \int K_{wr} sign(S_{wr})dt\right) \tag{3.51}$$

Then, Lyapunov stability condition is:

$$S_{wr}\dot{S_{wr}} = -\frac{S_{wr}}{J}\left(\lambda_{wr}|S_{wr}|^{\frac{1}{2}}sign(S_{wr}) + \int K_{wr}sign(S_{wr})dt\right) \tag{3.52}$$

And it becomes

$$S_{wr}\dot{S_{wr}} = -\frac{\lambda_{wr}}{J}|S_{wr}|^{\frac{3}{2}}sign(S_{wr}) - S_{wr}\frac{K_{wr}}{J}\int sign(S_{wr})dt \tag{3.53}$$

The stability condition is assured when both λ_{wr} and K_{wr} are positive, as observed from the negative nature of both terms in equation (3.53).

3.3 Simulation, Results, and Discussion

A numerical simulation was conducted under identical test conditions to showcase the enhancements achieved by implementing the suggested Direct Torque Control (DTC) with a first-order sliding mode controller, Twisting controller, and Super-Twisting controller. The ensuing figures depict various simulation diagrams corresponding to the aforementioned controllers.

3.3.1 Results of simulations

To demonstrate the performance of each controller, we initiate a consistent velocity of 1500tr/min for all three controllers. Subsequently, at 0.25 seconds, we apply a load torque of 6N.m.

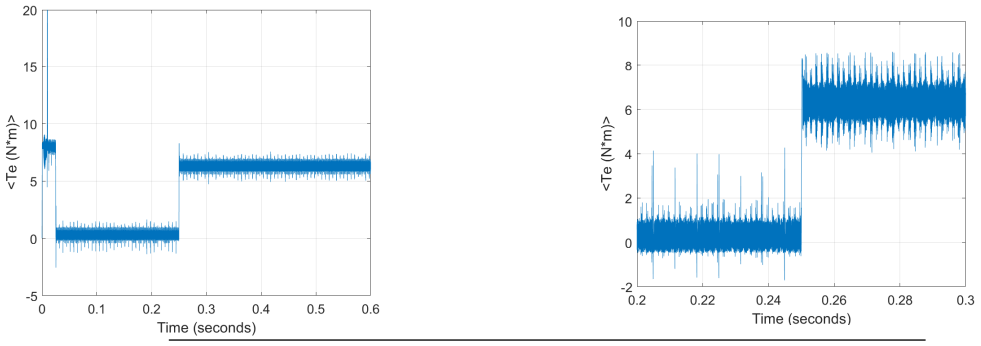

FIGURE 3.6: Torque response for 1st Order Sliding Mode

Since first order SMC is known for chattering and our machine already have high torque ripple, we can see that clearly in Figure 3.6. The system exhibits a peak torque during the transient period then it ranges from 2.1N.m to -1.27N.m. However, when the motor is loaded with 6N.m, the torque increases to approximately 7.6N.m to 5.3N.m.

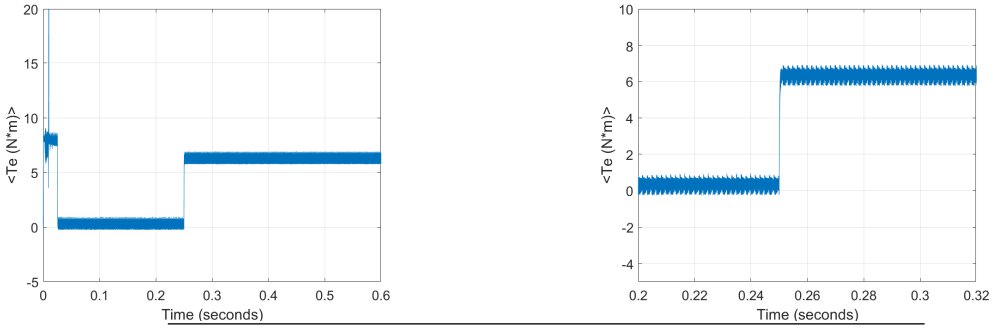

FIGURE 3.7: Torque response for Twisting controller

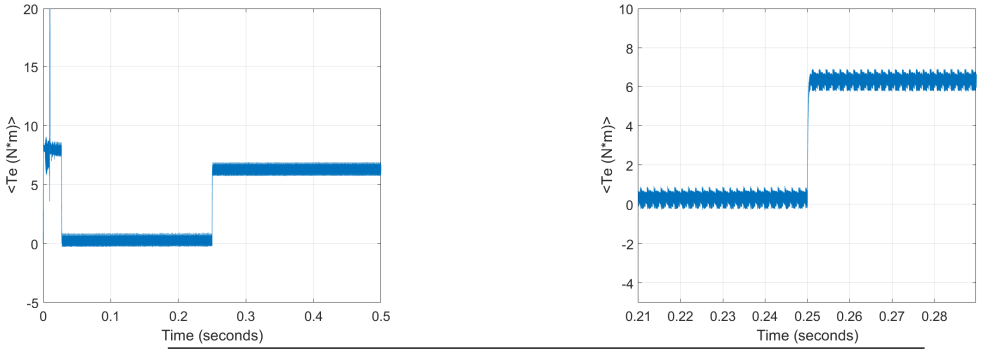

FIGURE 3.8: Torque response for Super-Twisting controller

When employing the Twisting controller (see Figure 3.7), the torque reaches its maximum value during the transient time and then settles between 0.937N.m to -0.268N.m in the steady state. After introducing a load of 6N.m, the torque rises to approximately 6.9N.m to 5.70N.m.

In the Super Twisting control scenario (shown in Figure 3.8), the torque exhibits a peak value during the transient period and subsequently stabilizes within the range of 0.8N.m to -0.25N.m in the equilibrium state. Upon the introduction of a 6N.m load, the torque increases to approximately 6.7N.m to 5.85N.m.

It is worth mentioning that the Twisting and Super Twisting controllers exhibit a substantial decrease in torque oscillation when compared to conventional regulation methods such as the PI and SM controllers.

The next figures (Figures 3.9-3.10-3.11) showcase the speed response for first order SM, Twisting, and Super Twisting controllers. We can see that first order SMC has robust performence but with the presence of overshoot. On the other hand, we clearly notice that with Twisting and Super Twisting controllers the speed response is very smooth compared to the first order SMC, there is only some difference in the speed drop where we see that the Super Twisting controller outperforms Twisting controller in the drop rate which is very important in our case.

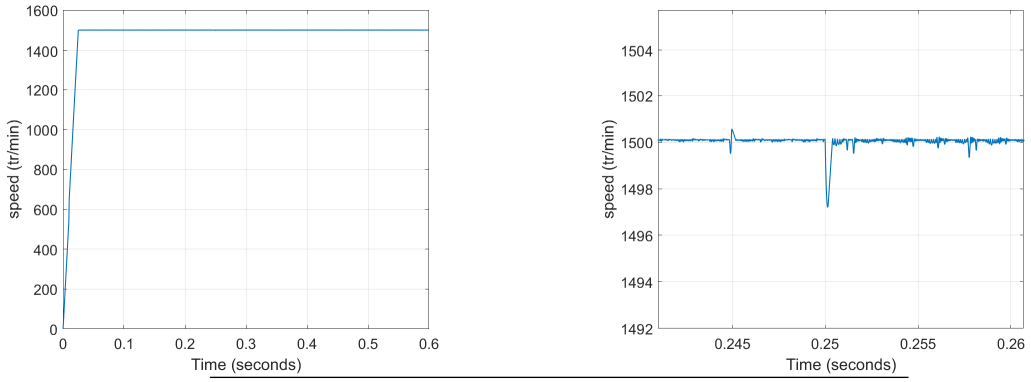

FIGURE 3.9: Speed response for 1st Order Sliding Mode

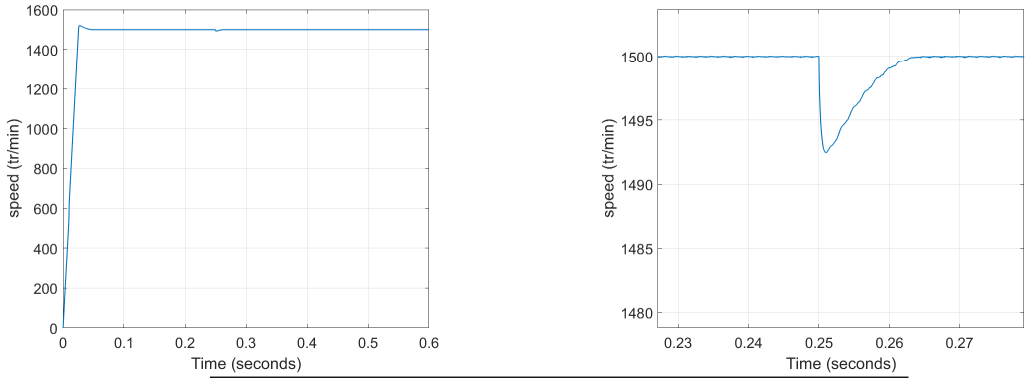

FIGURE 3.10: Speed response for Twisting controller

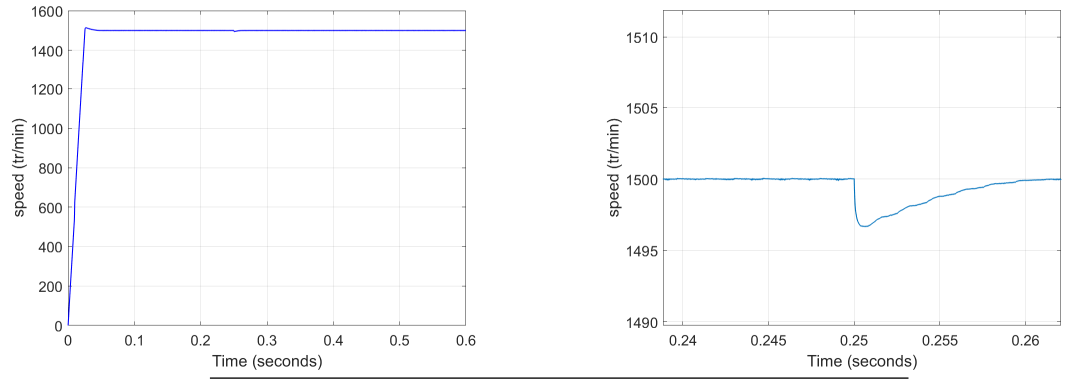

FIGURE 3.11: Speed response for Super-Twisting controller

To compare the results of all controllers we are going to present them together at the same figure then discuss those results.

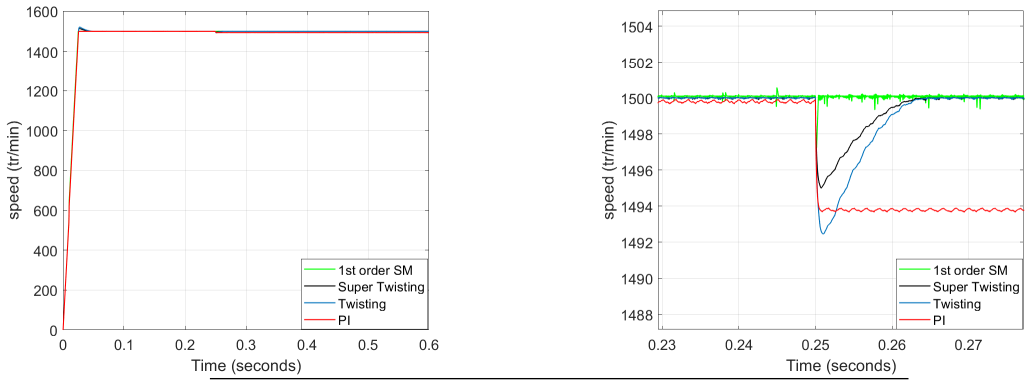

FIGURE 3.12: Speed PI/1st order SM/Twisting SM/Super Twisting SM

The provided graph (Figure 3.12) illustrates the performance of different controllers: PI, 1st order SMC, Twisting SMC, and Super Twisting SMC. It is evident that the Super Twisting SMC controller outperforms the other three controllers in terms of speed, steady state, and dynamic state responses.

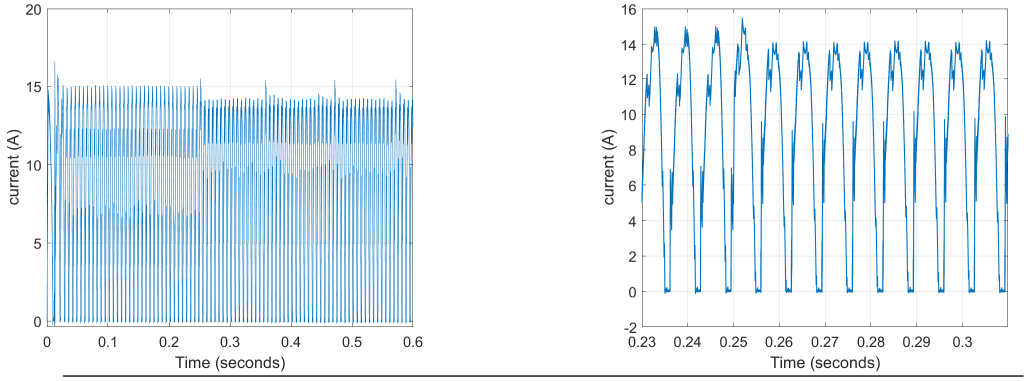

FIGURE 3.13: Output current ripple of one phase for First Order Sliding Mode

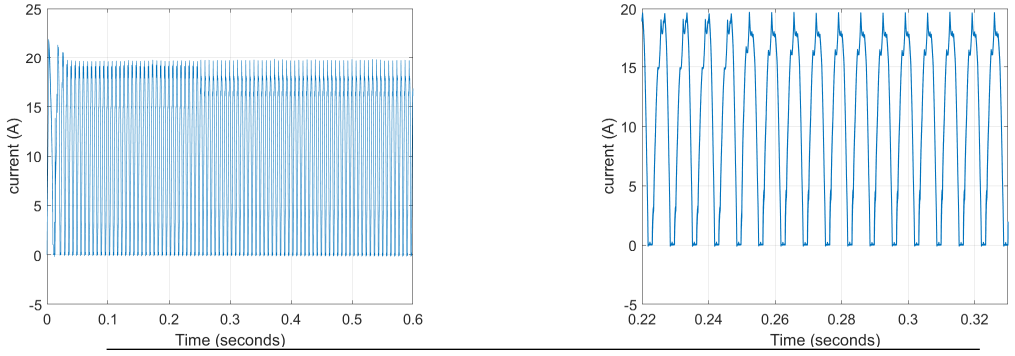

FIGURE 3.14: Output current ripple of one phase for Twisting controller

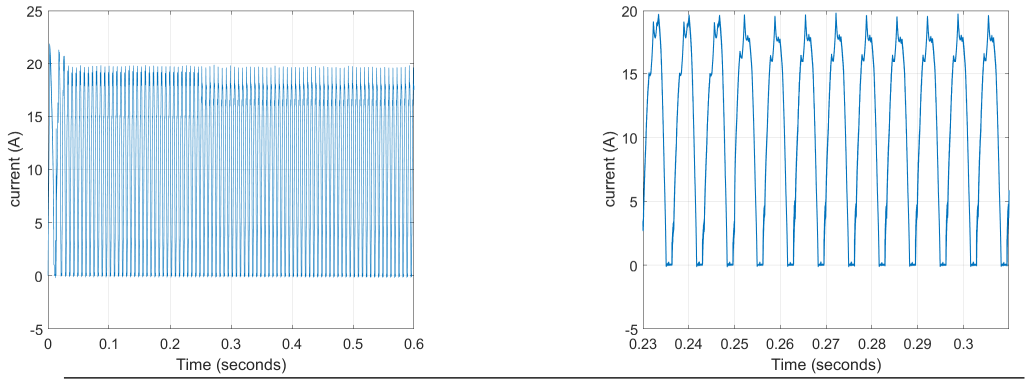

FIGURE 3.15: Output current ripple of one phase for Super-Twisting controller

In the case of Twisting and Super Twisting techniques (Figures 3.14-3.15), the current reaches its peak during the transient period and eventually stabilizes at around 20A in the steady state. After introducing a torque load, the current increases by approximately 0.5 to 1A. However, with the 1st order sliding mode, the current peaks initially and then stabilizes at 15A, which subsequently decreases to nearly 14A after applying the load torque. It is evident that both twisting and super twisting methods exhibit a smooth current profile, while the first order sliding mode demonstrates the presence of chattering phenomena.

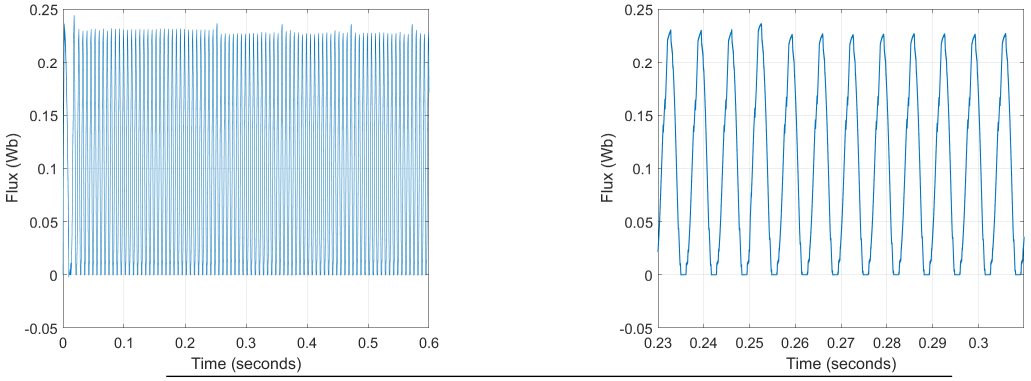

FIGURE 3.16: One phase flux linkage for 1st Order Sliding Mode

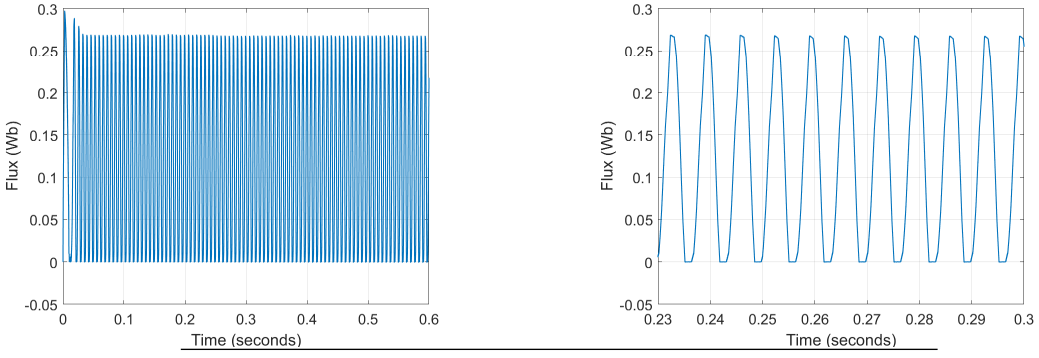

FIGURE 3.17: One phase flux linkage for Twisting controller

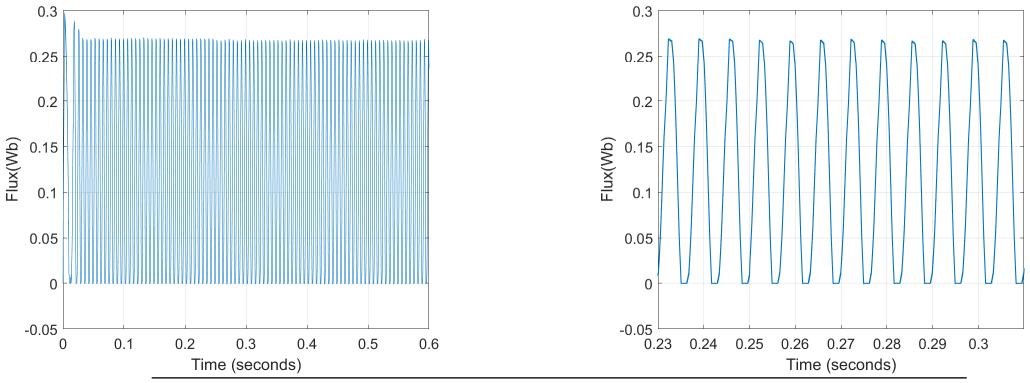

FIGURE 3.18: One phase flux linkage for Super-Twisting controller

The magnetic flux reaches its maximum value during the transient period and then stabilizes at 0.267Wb in the steady state, regardless of motor loading. We observe the remarkable smoothness of the flux for both Twisting and Super-Twisting controllers, particularly on the left side, when compared to 1st Order Sliding Mode.

A comparison study of the different control techniques is summarized in this table.

TABLE 3.1: The different performances of each controller

	Torque Ripple	Dynamic Response	Overshoot	Speed Drop (rpm)
DTC with PI	25%	0.035s	15%	6.2
DTC with 1st order SMC	38%	0.025s	30%	2 with overshoot
DTC with TwistingSMC	19%	0.02s	None	7.3
DTC with Super Twisting SMC	14%	0.02s	None	4.8

The methods of Direct Torque Control (DTC) PI, DTC Twisting, and DTC Super Twisting demonstrate rapid and efficient responsiveness. However, the overshoot observed in the case of TC and STC is comparatively lesser than that of PI and 1st order SMC. Additionally, the torque ripple in TC and STC is minimal when compared to the ripple experienced in PI and 1st order SMC.

3.4 Conclusion

This chapter provides a comprehensive explanation of the design process for three nonlinear controllers, namely SMC, TC, and STC, applied to the SRM system. Through a comparative analysis of simulation studies, it can be inferred that the Super Twisting control method

significantly enhances the drive speed regulation. Specifically, the Super Twisting controller demonstrates impressive performance in mitigating load torque disturbances and effectively reducing torque ripple caused by chattering.

Conclusion & Future Plans

This report explores robust Direct Torque Control (DTC) methods, specifically sliding mode control (SMC), Twisting controller (TC), and Super Twisting controller, for Switched Reluctance Motors (SRMs). The objective is to minimize torque ripples in SRMs. SRMs are popular in automotive, renewable energy, aerospace, and domestic appliances sectors due to their cost-effectiveness and simple rotor structure. However, they suffer from high levels of noise and vibration. The study addresses non-linearities and parameter uncertainties in SRM control and emphasizes the need for powerful and robust techniques. Sliding mode control proves to be a suitable solution, although the issue of chattering requires the application of Twisting and Super Twisting control for SRM control.

In this particular context, we initially provided an overview of the Switched Reluctance Motor (SRM), including its description, modeling, and supply.

Moving on to the subsequent chapter, we discussed the theory behind the conventional Direct Torque Control (DTC) as applied to SRM. This approach proved effective in achieving satisfactory performance in terms of tracking and regulation. The simulation results further supported the effectiveness of vector control for SRM.

Lastly, we have detailed the development of a sliding mode controller (SMC) for SRM. In order to mitigate chattering phenomena, we introduced the concept of Twisting and Super Twisting algorithm controllers for SRM drive. The validity of this proposal was confirmed by presenting simulation results.

The research conducted in this thesis presents several potential avenues for further exploration, specifically:

- Consider employing an alternative control approach, such as the implementation of Synergetic control.
- Using SRM in electric vehicle propulsion.
- The utilization of alternative control methods, such as adaptive control and contemporary control techniques (such as feedback linearization and backstepping).
- Sensorless control for SRM.

APPENDICES

Motor Parameters

Stator poles	8
Rotor poles	6
Phases	4
Input voltage	220V
Stator resistance	1.4Ω
Inertia	0.0011 $kg.m^2$
Friction	0.002 N.m.s
Turn on angle	45°
Turn off angle	75°
Estimated speed	1500 tr/min

Gains of Controllers

PI	$K_p = 0.15$ $K_i = 1.2$
First order SMC	$K_{wr} = 1.1$
Twisting controller	$K_1 = 1.3$ $K_2 = 0.5$
Super Twisting Controller	K_{wr} = -200 λ_{wr} = -2

Bibliography

[1] T. J. E. Miller, "Optimal design of switched reluctance motors,"IEEE Trans. Ind. Electron., vol. 49, no. 1, pp. 15-27, Feb. 2002.

[2] A. L. M. d. Santos, J. Anthonis, F. Naclerio, J. J. C. Gyselinck, H. V. d. Auweraer and L. C. S. Goes, "Multiphysics NVH modeling: simulation of a switched reluctance motor for an electric vehicle," IEEE Trans. Ind. Electron., vol. 61, no. 1, pp. 469-476, Jan. 2014.

[3] Ma, X.Y., Li, G. orcid.org/0000-0002-5956-4033, Jewell, G.W. et al Performance comparison of doubly salient reluctance machine topologies supplied by sinewave currents. IEEE Transactions on Industrial Electronics, 63 (7). 7437424. pp.4086-4096, 2016. ISSN 0278-0046.

[4] V. Shah, M. Alam and S. Payami, "High Torque/Ampere Direct Torque Control of Switched Reluctance Motor Drives," 2019 National Power Electronics Conference (NPEC), 2019, pp. 1-6.

[5] Kiran Srivastava, B. K. Singh, K.V. Arya, R.K.Singh."Simulation and Modeling of 8/6 Switched Reluctance Motor using Digital Controller". International Journal of Electronics Engineering, 3 (2), 2011, pp. 241– 246

[6] Wadnerkar, Vikas Das, G. Rajkumar, A. "Performance analysis of switched reluctance motor; design, modeling and simulation of 8/6 switched reluctance motor". journal of theoretical and applied information technology © 2005 - 2008

[7] Mohamad Abd Elmutalab ."Extending the speed range of a switched reluctance motor using a fast demagnetizing technique". Master Thesis, University of Akron. 2016

[8] Saman, Abbasian." Simulation and Testing of a Switched Reluctance Motor By Matlab /Simulink and dSPACE". Master Thesis Sweden, 2013.

[9] Skvarenina, T., 2002. The power electronics handbook. 1st ed. New York: CRC press, pp.400-410. [10] ARDESHIR, MOTAMEDI-SEDEH." SPEED CONTROL OF SWITCHED RELUCTANCE MOTORS". Master Thesis, Queen's University Kingston, Ontario, Canada,March 1998.

[11]R. Krishnan."SWITCHED RELUCTANCE MOTOR DRIVES Modeling, Simulation, Analysis, Design, and Applications" .p 38-41, 2001 by CRC Press LLC

[12]G. Fang, F. P. Scalcon, D. Xiao, R. P. Vieira, H. A. Gründling and A. Emadi,

"Advanced Control of Switched Reluctance Motors (SRMs): A Review on Current Regulation,Torque Control and Vibration Suppression," in IEEE Open Journal of the Industrial Electronics Society, vol. 2, pp. 280-301, 2021

[13] Adrian David Cheok and Yusuke Fukuda " A New Torque and Flux Control Method for Switched Reluctance Motor Drives" IEEE Transaction on Power Electronics. Vol. 17, No. 4 ,July 2002, pp.543-557

[14] FAHMY M EL-KHOULY. "High performance direct torque control of switched reluctance motor drives". Electric Power Components and Systems, 33(3) :287297,2004.

[15] Mokhtari , Bachir. "DTC INTELLIGENTE APPLIQUÉE À LA COMMANDE DE LA MACHINE ASYNCHRONE", Thèse de Doctorat en Sciences, Université de Batna, Algérie, 2014.

[16] S. Fahas, Hoang Le-Huy and I. Kamwa, "Fuzzy direct torque control of switched reluctance motors," IECON 2012 - 38th Annual Conference on IEEE Industrial Electronics Society, 2012, pp. 1811-1816

[17] A, DASH." DIRECT TORQUE CONTROL OF SWITCHED RELUCTANCE MOTOR DRIVES", Master Thesis ,NATIONAL INSTITUTE OF TECHNOLOGY, ROURKELA, INDIA,2014

[18] S,Gdaim. " Commande directe de couple d'un moteur asynchrone à base de techniques intelligentes". Thèse de Doctorat en Sciences, Ecole Nationale d'Ingénieurs de Monastir. Tunisia, 2013.

[19] B. Jeong, K. Lee, et al. "Direct torque control for the 4-phase switched reluctance motor drives". in: Proceedings of the 2005 IEEE International Conference on Electrical Machines and Systems, ICEMS 2005, 2005, 524–528.

[20]Fukuda. "A new torque and flux control method for switched reluctance motor drives". IEEE Transactions on Power Electronics, 2002, 17(4): 543–557.

[21] GUETTAF, Abd-erazek."Contribution à la conception de la machine à réluctance variable en vue de sa commande. Masters thesis", Université Mohamed Khider Biskra. (2005)

[22] Y,Saadi. " Stratégies de contrôle et analyse des défauts d'une machine à réluctance variable pour une chaîne de traction électrique ". Automatique / Robotique. Université Paris Saclay.2019.

[23] Jinkun,Liu." Sliding Mode Control Using MATLAB".by Academic Press, 2017.pages 81- 96.

[24] A. Levant, "Higher-order sliding modes, differentiation and output feedback control," Int. J. Control, vol. 76, no. 9-10

[25] X. Rain, M. Hilairet and R. Talj, "Second order sliding mode current controller for the switched reluctance machine," IECON 2010 - 36th Annual Conference on IEEE Industrial Electronics Society, Glendale, AZ, USA, Nov. 2010, pp. 7–10.

[26] SAIBI, Hayat.KASSOURI, Dalila. “Commande par mode glissant d’ordre fractionnaire d’un réseau électrique”. Master Thesis. Université Mouloud MAMMERI, Tizi-Ouzou

[27] M,Manceu .’Commande robuste des systemes non lineaires complexes’. THESE de Docteur. 2012

[28] A. Faqir, F. Betin, L. Chrifi Alaoui, B. Nahid and D. Pinchon, ”Varying sliding surface control of an SRM drive”, in IEEE Conference on Control Applications Proceedings, 2003

[29]Vadim, Utkin. Hoon, Lee.”CHATTERING PROBLEM IN SLIDING MODE CONTROL SYSTEMS”.IFAC Proceedings Volumes,Volume 39.’ Issue 5.2006.Page 1.ISSN 1474- 6670,ISBN 9783902661067.

[30]Vadim, Utkin. Jürgen, Guldner. Jingxin, Shi. “Sliding Mode Control in electromechanical systems”. Boca Raton, Imprint CRC Press,2017. Page 172

[31]Utkin, V., Guldner, J., Shi, J.”Sliding Mode Control in Electro-Mechanical Systems (2nd ed.)”. CRC Press. (2009). https://doi.org/10.1201/9781420065619

[32] Deghboudj, Imen.” COMMANDE DES SYSTEMES NON LINEAIRES PAR MODE GLISSANT D’ORDRE SUPERIEUR”. Magister Thesis, University Constantine, 2013

[33]Y,Shtessel.Ch,Edwards.L,Fridman.A,Levant. “Sliding Mode Control and Observation”. New York, NY,2014.page 145-148

[34] J,Slotine .L,Weiping.” applied nonlinear control”. Prentice Hall, Englewood Cliffs, New Jersey, 1991.pages 285-287

[35] Muhammad Rafiq Mufti, Qarab Raza Butt, S. Iqbal, M. Ramzan, ”Position Control of Switched Reluctance Motor Using Super Twisting Algorithm”, Mathematical Problems in Engineering, vol.2016, https://doi.org/10.1155/2016/9658967

[35] A. Levant, ”Higher-order sliding modes, differentiation and output-feedback control”, International Journal of Control, vol. 76, no. 9-10, pp. 924-941, 2003.

[36] BENDAAS Ismail “Contribution à la Commande Hybride par Mode Glissant Floue. Apport des Techniques de L’intelligence Artificielle” Ph.D. thesis, University of Batna, Algeria,2016.

[37] Bartolini, G.; Ferrara, A.; Usai, E. Chattering avoidance by second order sliding mode control. IEEE Trans. Autom. Control 1998, 43, 241–246.

[38] M. Rashed, K. Goh, M. Dunnigan, P. MacConnell, A. Stronach and B. Williams, ”Sensorless second-order sliding-mode speed control of a voltage-fed induction-motor drive using nonlinear state feedback”, IEE Proceedings -Electric Power Applications, vol. 152, no. 5, p. 1127, 2005.

[39] J. Hung, W. Gao and J. Hung, ”Variable structure control: a survey”, IEEE Transactions on Industrial Electronics, vol. 40, no. 1, pp. 2-22, 1993